11

Ultrafast Laser Pulse Synchronization

Heping Zeng, Ming Yan and Wenxue Li
State Key Laboratory of Precision Spectroscopy
East China Normal University
China

1. Introduction

Progress in ultrafast science and technology has pushed the temporal resolution to sub-femtosecond and attosecond region (Kienberger el at., 2002; Fleischer & Moiseyev, 2006; Corkum & Krausz, 2007; Goulielmakis el at., 2007) and technology exploration in ultrashort pulse generation has made it possible to equip femtosecond lasers that are only a few cycles in duration (Xu el at., 1996; Shirakawa el at., 1999; Rullière, 2005; Mauritsson el at., 2006; Sansone el at., 2006). Coherent control experiments now use precisely shaped optical pulses with sub-femtosecond timing jitters to steer coherent evolution governed by the interaction of coherent light with matter towards quantum paths for desired dynamic processes (Kitzler el at., 2002;Tong el at., 2003; Bandrauk el at., 2005). Precise control and synchronization of ultrashort pulses are essential for many other applications in ultrafast laser spectroscopy (Drescher el at., 2002; Hannaford, 2005; Cavalieri el at., 2007), Fourier synthesis of light pulses or optical waveforms (Jones el at., 2000; Shelton el at., 2001; Supradeepa el at., 2008), multi-color pump-probe investigations (Schoenlein el at., 2000; Son el at., 2002; Manzoni el at., 2006; Gu el at., 2009), coherent anti-Stokes Raman scattering microscope (Jones el at., 2002; Potma el at., 2002), difference frequency mixing for mid-infrared generation (de Barros el at., 1995; Kaindl el at., 2000) and terahertz source generation (Kitaeva, 2008; a. Sell el at., 2008; b. Sell el at., 2008), and so forth. Recently, significant breakthrough has been made in ultrafast laser technology and precision frequency metrology (Hentschel, el at., 2001;Udem el at., 2002; Schibli el at., 2004) with the innovation concept of simultaneous control in both time and frequency domain developed in femtosecond combs (Shelton el at., 2001; Ma el at., 2004). This technique is versatile in controlling ultrashort mode-locked lasers by translating precision control over mode frequencies into ultra-stable control in the time domain, which may eventually facilitate accurate synchronization of multicolor mode-locked lasers desired for coherent optical synthesis to extend the pulsed laser spectrum (Jones el at., 2000; Shelton et al., 2001; Bartels el at., 2004).

Rapidly growing interest has been focused in recent years on synchronizing independently mode-locked multi-color lasers with improved synchronization accuracy and robustness, sufficiently low time jitters, as well as large tolerance to disturbance (Kawamura el at., 2000; Rudd el at., 2005; Baudelet el at., 2006). In general, pulse synchronization requires independent lasers to be mode-locked at exactly the same repetition rate. As the repetition rate (f_r) depends linearly on the effective cavity length (L_{eff}), $f_r=c/L_{eff}$ (c, the speed of light in vacuum), a feed-back locking system is indispensible for laser synchronization to compensate for the unavoidable cavity variations. In accordance with the feedback methods,

laser synchronization scheme can be classified into active, passive and hybrid synchronization. In the active synchronization scheme, the feedback is typically provided by electronic phase-locking-loop devices (Schibli el at., 2003), which offer the advantage of long-term stability and independence on the oscillating wavelengths in laser operation. However, such a scheme suffers from limited bandwidth of electronic circuits and the time jitter among synchronized lasers is critically dependent on the control precision of the electronic circuits. Passive synchronization is typically achieved by using all-optical methods on the basis of nonlinear optical effects within the concerned laser cavities (Bartels el at., 2003; Yoshitomi el at., 2006). Although the passive technique is limited by the walk-off length of the synchronous lasers, it provides relatively simple laser configurations and in most cases, results in small timing jitters, making it attractive and popular in laser synchronization experiments. Besides active and passive synchronization schemes, the active-passive hybrid synchronization technique combines the advantages of the both schemes (Yoshitomi el at., 2005). The walk-off length of the synchronous lasers is reduced by using active feedbacks with electronic phase-locking-loop devices, while small time jitters among synchronized lasers are guaranteed by nonlinear optical couplings within the synchronizing laser cavities. Correspondingly, the hybrid synchronization scheme becomes more complicated than the other two schemes.

The stabilization of the synchronization between separate lasers depends critically on cavity length mismatch. With large cavity length mismatch tolerance, a synchronized laser system can be expected to work stably in tough environments. In principle, cavity length variations (ΔL) and offset frequency drifts (Δf_r) between different lasers can be effectively balanced by modulating the intracavity dispersion and nonlinearity. For instance, the cavity length mismatch can be effectively compensated by cross phase modulation (XPM) effect. By this means, synchronous mode-locking can be achieved in coupled-cavity lasers by sharing the same Kerr-type nonlinear medium (Wei el at., 2002), or by injecting the master laser pulses into the slave laser in the master-slave configuration for independently mode-locked lasers (Yoshitomi el at., 2006). Until now, a record cavity length mismatch about 140 μm was realized in master-slave fs fiber lasers (a. Rusu el at., 2004). However, it should mention that in the coupled-cavity lasers, a large length variation of the coupled cavity may destabilize the mode-locking and pulse-train synchronization. Once the cavity lengths are largely mismatched in comparison with the walk-off length, XPM-based passive schemes may fail in enforcing synchronous mode-locking. Since XPM is limited within the walk-off length between the interacting pulses, high peak powers are required to induce sufficient optical nonlinearity for a tight synchronization. Furthermore, in the master-slave laser injection configuration, the injection power of the master laser is seriously limited by the light coupling equipments like the fiber coupler, the wavelength-division multiplexing (WDM), Lens and mirrors, and so on. Therefore, the relatively low-intensity master pulse can only induce limited wavelength shifts and round-trip group delay changes for the slave laser catching up with the master laser pulses. To achieve a large cavity mismatch tolerance, a hybrid configuration with the master-slave and the coupled-cavity schemes is recommended. The hybrid passive synchronization scheme entails XPM an additional function in the slave laser to start mode-locking rather than merely to shift the central wavelength and modulate the intracavity group delay, from which influences of the master laser injection can be greatly enhanced. As a consequence, XPM mode-locking in the hybrid master-slave configuration exhibits advantageous features inherited from both coupled-cavity and master-slave schemes, i.e., remote control of slave lasers with independently mode-locked master lasers, sensitive influence of the master injection on XPM mode-locking.

It is of broad interest to synchronize pulses of variable pulse durations from fs to ns. Nanosecond laser pulses are typically obtained by Q-switching techniques and synchronized by external electronic triggering with timing jitters in the ns range. It is still a technical challenge to construct coherent ns-duration pulse arrays with an ultrahigh resolution in the time domain due to the lack in efficient techniques for precise temporal and spectral control of ns pulses. All the synchronization schemes developed so far are inapplicable for coherent phase-locking of ns optical pulses. On the other hand, high-energy ns lasers precisely synchronized with the same triggering fs laser could support the development of phase-locked high-energy ns laser arrays for promising applications in particle acceleration and fast ignition (Kodama el at., 2001), and ultrashort laser synchronization with x-rays or electron beams from synchrotrons (Schoenlein el at., 2000). Furthermore, fs laser synchronization with a high-energy ns laser could facilitate lasers of different pulse durations to interact with the target under a precise control in the time domain (Kodama el at., 2001; Vozzi el at., 2009), which is also quite useful for the development of robust and stable optical parametric chirped pulse amplifiers (Butkus el at., 2004; Rudd el at., 2005; Zhang el at., 2006). It has been recently demonstrated that square ns mode-locking could be established in a fiber laser of a long fiber cavity (Potma el at., 2002), and that the square ns pulses could be scaled to hundred watts with negligible temporal and spectral distortion by using large-mode-area fiber amplifiers (b. Yan el at., 2009). Interestingly, square ns mode-locking could be passively synchronized with an ultrashort laser in the master-slave laser configuration (Li el at., 2009). Since the long fiber cavity indispensable for square ns mode-locking typically produces a large cavity length variation, sufficiently strong master injection pulses are required to trigger a synchronous square ns mode-locking of the slave laser (Vozzi el at., 2009). A large cavity mismatch tolerance is especially required for the precise control over mode frequencies in a long fiber cavity that allows synchronized square mode-locking in the ns region.

In this chapter, we review our recent experimental development in synchronizing multicolor mode-locked fiber lasers of different pulse durations. A robust technique based on cross-absorption modulation (XAM) was demonstrated efficiently for ultrashort fiber laser synchronization in the master-slave configuration. For fiber lasers mode-locked through nonlinear polarization rotation (NPR) in the fiber laser cavity, XAM induced an observable change of the NPR in the slave fiber laser cavity due to the nonlinear couplings between the slave laser pulses and the externally injected fs master laser pulses, resulting in a trigger for square ns mode-locking in slave fiber laser that generated ns output pulses of square temporal profiles with the pulse duration dependent linearly on the master injection power. Square ns mode-locking synchronized with a fs Ti:sapphire master laser was achieved in both Yb- and Er-doped slave fiber lasers by using additional Er-doped fibers as the saturable absorber. The synchronization of the square ns pulses with the fs master injection was implemented with the rising edges of the ns pulses tightly synchronous to the injected fs pulses, with remarkably low time jitters in the range of hundreds femtoseconds. Furthermore, such an XAM-based synchronization could be maintained with the record cavity-length mismatches exceeding 8.2 and 3.6 cm for the Yb- and Er-doped slave fiber lasers, respectively. Interestingly, the XAM-based synchronization could be used to synchronize mode-locked lasers at a relatively low repetition rate of sub-MHz (a. Yan el at., 2009; b. Yan el at., 2009), while the square ns mode-locked laser pulses could be controlled to output tunable flat-top pulses with the pulse rising edges tightly synchronized with the triggering fs pulses, and high-power amplification could be realized by using large-mode-area photonic crystal fiber amplifiers for the synchronized pulses. The synchronized square

ns pulses could be easily controlled by varying the master injection power, confirming that the square ns mode-locking worked with observable intra-cavity power clamping and that the clamped power in the slave fiber laser could be varied by XAM-induced changes of the optical nonlinearity of the Er-doped fiber. Note that the square ns pulses were controlled by this synchronous mode-locking method with an ultrahigh temporal resolution at least four orders of magnitude better than the corresponding pulse duration. As a result, the synchronously triggered square ns mode-locking provides a robust method not only for the precise control of the square ns pulses in the time domain, but also for the convenient experimental realization of synchronized pulses variable from fs to ns in pulse duration.

This review chapter is organized as follows. After this brief introduction, we present the basic theory for passive synchronization in Section 2. Section 3 mainly compares XPM- and XAM-based synchronization schemes applicable for ultrafast laser synchronization and square nanosecond mode-locked laser synchronization. The amplification of synchronous high-energy laser pulses is discussed at the end of this section. We conclude the review in section 4 by emphasizing that the XAM-based synchronization technique is a promising supplement to the XPM-based passive synchronization.

2. Basic theory for XPM- and XAM-based synchronization

Nonlinear effects in a Kerr medium or in fiber competing with light dispersion within the laser cavity provide an effective feed-back effect for laser pulse going against cavity variation and staying at a same repetition rate (or round-trip frequency) with another laser. Thus, to analyze passive synchronization mechanism, we need start with the nonlinear effects like cross-phase modulation and cross-absorption modulation. An established XPM theory has been reported for several decades, while very few information about XAM is reported. In this Section, we concentrate on the detailed discussion of the XPM-based passive laser synchronization, and introduce some basic understanding about the XAM-based synchronization under investigation.

2.1 Cross phase modulation

To analyze the supporting role of cross-phase modulation in passive synchronization, we assume that two lasers (laser-1 and laser-2) share the same nonlinear medium with a given length of L inside their cavities. The nonlinear refractive index for this medium is denoted as n_2. Before being synchronized, the two lasers can be independently mode-locked to produce ultrashort pulse trains at different center wavelengths. The round-trip frequencies for laser-1 and laser-2 are f_1 and f_2, respectively. Therefore, the two laser pulses can meet each other in the nonlinear medium with a frequency of $\Delta f = |f_1 - f_2|$. Once the two pulses co-propagate inside the shared medium, there exists a possibility for the two lasers to run at the same round-trip frequency as the nonlinear couplings may produce offset frequency drifts so that different lasers can be effectively matched. Assume that $E_1(z,t)$ and $E_2(z,t)$ represent the envelope of the electric field of laser-1 and -2, respectively. Since the two pulses have different wavelengths as well as different group velocities (v_{G1} and v_{G2}), the two pulses will co-propagate in the medium within a walk-off length of $L_{off} = \frac{T_1}{d}$, where $d = \frac{(v_{c1} - v_{c2})}{v_{c1} v_{c12}}$ and T_1 is the pulse duration of Laser-1 at the starting position of interaction region. If $L > L_{off}$, the

pulse interaction inside the nonlinear medium can be theoretically expressed in terms of the nonlinear propagation equations as (a. Agrawal, 1989; Zhu el at., 2005):

$$\begin{aligned}&\frac{\partial}{\partial z}E_1(z,t)+d\frac{\partial}{\partial t}E_1(z,t)+i\frac{\beta_1}{2}\frac{\partial^2}{\partial t^2}E_1(z,t)+\alpha_1 E_1(z,t)\\&=i\gamma_1\left[|E_1(z,t)|^2\,E_1(z,t)+2|E_2(z,t)^2E_1(z,t)\right],\end{aligned}\tag{1}$$

$$\begin{aligned}&\frac{\partial}{\partial z}E_2(z,t)+d\frac{\partial}{\partial t}E_2(z,t)+i\frac{\beta_1}{2}\frac{\partial^2}{\partial t^2}E_2(z,t)+\alpha_2 E_2(z,t)\\&=i\gamma_2\left[|E_2(z,t)|^2\,E_2(z,t)+2|E_1(z,t)^2E_2(z,t)\right],\end{aligned}\tag{2}$$

where z and t denote the laser pulse propagation distance and time. Subscripts 1 and 2 denote the laser-1 and -2. a is the linear absorption coefficients, β is the intra-cavity group velocity dispersion (GVD), and $\gamma=2\pi n_2/(\lambda A_{eff})$ is the nonlinear coefficient, where A_{eff} is the effective beam cross section and λ is the center wavelength. In these equations, the contribution of GVD is described by the third term on the left-hand side. As to the right-hand side, the first term is due to the self-phase modulation (SPM) effect and the second term for the XPM effect. By analytically resolving these two equations, one can finally get soliton-like solutions (Baldeck el at., 1988; Agrawal el at., 1989).

For the sake of simplicity, we merely consider the effects of GVD and XPM while omitting the influence from the self-phase modulation. As a result, the maximum phase shift $\Delta\varphi_{21}$ of laser-1 induced by laser-2 can be expressed as (Lisak el at., 1990):

$$\Delta\varphi_{21}=\frac{\gamma_1 P_2 L_{off}}{\pi T_1},\tag{3}$$

and correspondingly, the laser-1 induced maximum phase shift $\Delta\varphi_{12}$ to laser-2 is:

$$\Delta\varphi_{12}=\frac{\gamma_2 P_1 L_{off}}{\pi T_2},\tag{4}$$

where P is the peak power of laser pulse.

In order to understand the feed-back mechanism of XPM effect in passive synchronization, we need consider the XPM-induced phase shift in frequency domain. Supposing the laser-1 and -2 having instantaneous optical frequencies of ω_1 and ω_2, respectively, the XPM-induced frequency change can be simply described as (Wei el at., 2002):

$$\Delta\omega_1\propto -n_2\frac{\partial I_2}{\partial t},\tag{5}$$

$$\Delta\omega_2\propto -n_2\frac{\partial I_1}{\partial t},\tag{6}$$

where I is the intra-cavity laser intensity. In general, the two lasers have a quite similar round-trip frequency, but not exactly equal. The relative fluctuation Δf for the two lasers may come from any small perturbations during the laser operation, such as small cavity-

length drifts, thermal and temperature fluctuation, random polarization change, pump instability and so on. As affected by the perturbations, the initially co-propagated laser-1 may go behind or ahead of the laser-2, as shown in Fig. 2-1.

In the case that the laser 1 goes behind the laser 2, the rising-edge of laser-1 will cross with the falling-edge of laser-2. Because the slope of intensity I_2 is negative in its falling-edge for laser-1, the spectrum of laser-1 will be blue-shifted ($\Delta\omega_1>0$) while laser-2 will be red-shifted ($\Delta\omega_2>0$) due to the positive intensity slope of I_1, according to relation (5) and (6). Thus, in a medium with negative group dispersions for the two lasers, the blue-shifted light will go

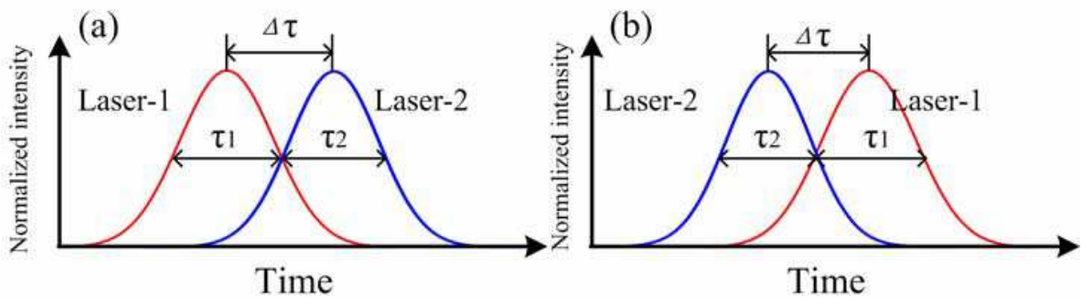

Fig. 2-1. The propagation schematic diagram of Laser-1 (a) behind and (b) ahead Laser -2.

faster than the red-shifted one, and therefore the delayed pulse (laser-1) can catch up with the advancing pulse (laser-2). In the case that laser-1 is ahead of laser-2, the XPM will lead laser-1 to be red-shifted and laser-2 to be blue-shifted in spectrum, which may eventually make both pulses be maximally overlapped in the time domain. Once the pulses are maximally overlapped, the spectral shifts for both pulses will be reduced to zero, since the laser intensity profile is supposed to be temporally symmetric. In this situation, the two lasers operate at a synchronization state with the same round-trip frequency.

For evaluating a passive synchronization system, there are two crucial parameters: 1) the ability for the system compensating for environmental perturbations which is estimated by the value of cavity mismatch tolerance, and 2) the precision for the synchronization which is defined as timing jitter between the two laser pulses (Shelton el at., 2002). Besides, the synchronization stability is also an important factor to decide how long lasers are operated at synchronization state. Recently, experimental results have shown that the jitter for two separate fs pulses has been reduced into attosecond region and the mismatch tolerance is extended to several centimeters. The details for experimentally measuring these two parameters will be presented in Section 3-2.

As an automatic feed-back effect, XPM is considered to be an effective method to passively realize robust laser synchronization for last decades. However, XPM is not the only mechanism employed in synchronization scheme. Recently, a novel effect based on cross absorption modulation has been demonstrated quite useful and robust to synchronize two independently mode-locked lasers of ultra-long fiber cavity, which supports large cavity length mismatch tolerance. The next Section 2.2 will focus on the details of the XAM effect and its application background.

2.2 Cross absorption modulation

Cross absorption modulation was first reported in the Reference (a. Yan el at., 2009) for synchronizing a ytterbium-doped and a erbium-doped fiber lasers to an fs Ti:sapphire laser

at a repetition rate of nearly 240 kHz. It was well demonstrated that the cavity length mismatch could be compensated by XPM in coupled-cavity lasers sharing the same Kerr-type nonlinear medium, or independently mode-locked lasers in the configuration with master injection into the slave laser. However, XPM is limited within the walk-off length between the interacting pulses for purpose of synchronizing a fiber laser with an 800-m-long cavity (corresponding to a repetition rate of 240 kHz). This produces the technical challenge to passively synchronize ns-duration fiber lasers with an ultra-short laser. The long fiber cavity indispensable for square ns mode-locking produces a little difficulty to achieve a stable and robust passive synchronization. As the fiber cavity-length is much longer than the walk-off length, one cannot rely on XPM-based passive schemes.

Cross absorption modulation is a kind of modulation on slave light imposed by master light through a co-propagating medium which periodically absorbs the master light and then switches from its ground state to an excited state with a change of its refractive index or nonlinear coefficient. XAM is normally ignored in non-resonant interaction media as the nonlinear absorption coefficient is typically two-order smaller than the nonlinear coupling coefficient. Nevertheless, it may be comparable to or even larger than XPM in the near-resonant media.

In the resonant medium, the modulation can be enhanced by propagating pulse stimulating the medium from its ground state to an excited one. The enhanced XAM adjusts the group velocity of the co-propagating slave pulses through changing the nonlinear refractive index of the resonant medium to match the repetition rate of the slave laser with that of the master laser. Thus, the slave pulse polarization can be rotated owing to the changed nonlinear refractive index. For a mode-locked fiber laser, since the intra-cavity polarization state is changed, the temporal or spectral characteristics of the slave pulse must be also changed with the master laser. However, the instinct mechanism of XAM is under investigation and thus a systematic theory about XAM-based synchronization is still lack. In section 3.3 the novel XAM-synchronization will be described from the aspect of its experimental realization.

3. Passive synchronization techniques

As mentioned in the introduction part of this review chapter, active synchronization with an electronic feedback device suffers from the limitation of the timing jitters of detectors, filters, mixers and piezo transducers and so on (Spence el at., 1993; Crooker el at., 1996). Despite a record timing jitter of 300 as was achieved between Cr:Forsterite and Ti:Sapphire lasers by the active synchronization (Vozzi el at., 2009), the complexity of such an electronic system makes the technique unpopular. Unlike the electronically supported synchronization, passive technique permits an all-optical method to obtain synchronous laser pulses without the limitations from the complicated electronic feedback scheme. By the passive synchronization scheme (Yoshitomi el at., 2006), timing jitter of 3.7 fs was reported for synchronizing an Er-doped fiber laser to a mode-locked Cr:Forsterite. To date, a record timing jitter as low as 100 as has been achieved by using an active-passive hybrid synchronization scheme (Yoshitomi el at., 2005). Thus, the passive synchronization technique is concerned as an alternative or a co-operator for the active one. Most of these reported passive synchronization systems relay on XPM to modulate the intra-cavity dispersion and nonlinearity for matching the cavity lengths and offset frequency drifts of different lasers. Recently, the XAM-based technique has also been reported to be able to passively synchronize two lasers at a relatively low repetition rate of sub-MHz (a. Yan el at.,

2009). In this section, we will focus in what follows on various experimental implementations of these passive techniques. Section 3.1 aims at the precise XPM-synchronization for ultra-fast lasers at high repetition rate. Section 3.2 discusses an application of the XPM technique in the synchronization between ps and ns lasers. A mode-locked ns pulse generation technique will be also introduced in this section. After preliminary discussion on a few examples of different synchronization configurations, we present experimental measurements of the mismatch tolerance and the RMS timing jitter. Section 3.3 is concentrated on the XAM-based synchronization and its experimental results, while Section 3.4 concerns the synchronous pulse amplification and its impacts on the synchronization precision.

3.1 Accurate synchronization among ultra-fast lasers

During the last decades, the XPM effect has been employed as the major method to passively synchronize individually operated lasers. Such an XPM-technique can be realized (1) in a shared laser cavity or a shared nonlinear medium, or (2) in a master-slave injection configuration in which the two laser pulses interacted with each in a segment of single mode fiber inside the slave laser cavity. Usually case (1) appears in solid laser system. Since light intensity can be hardly improved to a large extent in free space, the required XPM is mainly provided by the large nonlinear coefficient of the shard medium. In this case, the two lasers play the equal role in synchronization and no distinction between master and slave laser. In this kind of synchronization scheme, the two lasers are cross-mode-locked at the same repetition rate (or round-trip frequency) to produce dual-wavelength laser light. As a distinct contrast with the case (1), the two lasers in case (2) show obviously distinguished roles as a master and slave laser. Generally, the slave laser is made by a fiber laser for a large intensity in constrained space and it oscillates dependently on the master laser, while the master works at a relatively independent state. The difference for the two cases is that case (1) is more sensitive to the environmental fluctuation while the construction of case (2) is much simple. In this Section, we will first introduce a fraction spectrum amplification technique to generate synchronous ultra-fast pulses. This technique is not widely used as XPM technique, but it can easily produce dual-wavelength pulses with ultra-low timing jitter in a certain situation. We will then give some particular examples to show how to experimentally obtain synchronous pulses with XPM technique in case (1) and case (2), respectively.

3.1.1 Synchronous pulses from fraction spectrum amplification

In many cases, there exists a situation that a mode-locked laser oscillator operates with non-continuous spectrum. In this case, the output of the oscillator can be spectrally separated into two (or more) parts: the main part (master source) is operating at λ_1 with spectral width of $\Delta\lambda_1$, and a small fraction (slave source) simultaneously works at λ_2 ($\lambda_2 \neq \lambda_1$) with spectral width of $\Delta\lambda_2$. Note that the two parts are spectrally separated but temporally overlapped. By spectrally detaching the two parts and amplifying the slave fraction, one can easily obtain two synchronous pulses centering at two different wavelengths. This method for obtaining synchronous pulses at various wavelengths is dubbed as fraction spectrum amplification (FSA). Since the two lasers come from the same cavity in FSA, the timing jitter between the two synchronous pulses can easily controlled to quite small values, even as small as sub-fs. As a typical example for FSA synchronous pulses generation, we introduce here a

synchronous FSA of a few-cycle Ti:Sapphire fs laser with the experimental setup as schematically illustrated in Fig. 3-1 (a. Li el at., 2009).

FSA is a useful way to generate synchronous pulse trains, but its realization requires a special laser source. The source used in this example is a commercialized Ti:sapphire laser oscillator (Rainbow). The specialty for this laser is that it deliveries fs pulse trains at a center wavelength of 800 nm with the spectral width of ~100 nm and at a near-IR fraction center of 1040 nm [shown in Fig. 3-2 (a)]. The 1040-nm light of 150 μW is much weaker than the 800-nm light of 200 mW. Considering the large difference in average power of the two parts, FSA becomes a favorable choice to easily realize synchronous pulses in this Ti:sapphire laser system. As the master source, the 800-nm light is temporally compressed into 10-fs region. And the 1040-nm fraction covering a spectra range from 980 nm to 1070 nm is employed as the slave source.

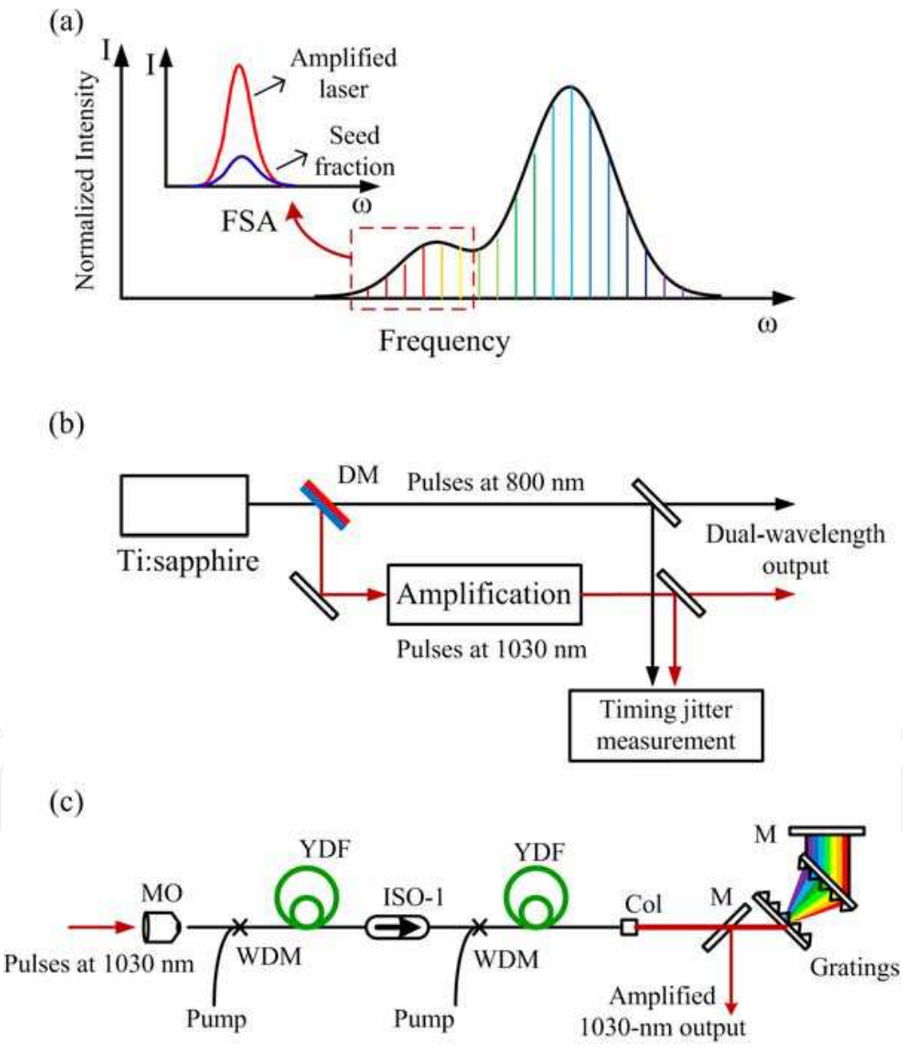

Fig. 3-1. (a) Spectral schematic of FSA, (b) experimental schematic of FSA and (c) experiment setup of the amplification section. MO, micro-objective; ISO, optical isolator; WDM, wavelength-division multiplexing (980/1064 nm); YDF, ytterbium-doped fiber; DM, dual-wavelength mirror.

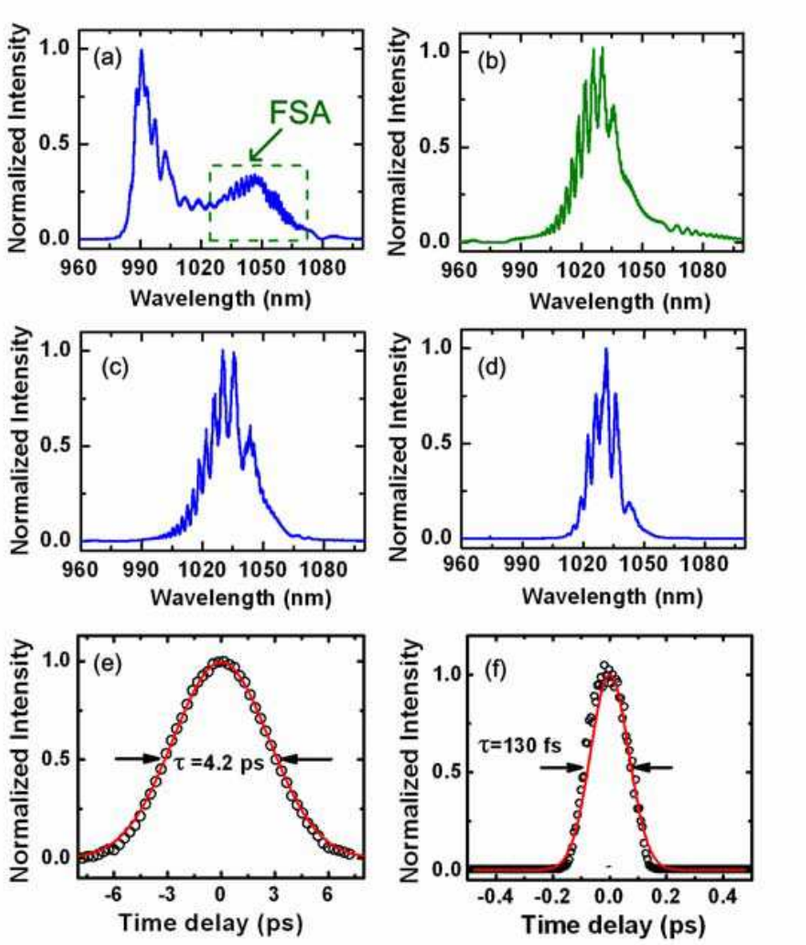

Fig. 3-2. The fraction spectrum of the few-cycle Ti:sapphire laser pulse (a), the gain spectrum of the Yb-doped fiber (b), the spectrum of the first-stage (c) and the second-stage (d) Yb-doped fiber amplifiers, the pulse duration of the amplified laser at 1030 nm before (e) and after (f) the grating compression.

The selection of amplifiers for the FSA is dependent on many factors such as the wavelength of the seed pulse, the setup complexity, the incident pulse power, gain bandwidth, and so on. By considering the near-IR spectral property and the weak power of the 1040-nm fraction source, ytterbium-doped fiber amplifier is recommended as an advantageous selection for amplifying such weak seed light pulses. As shown in Fig. 3-1 (c), a two-stage fiber amplification system is utilized for the FSA. It is difficult to directly amplify a weak signal into high power by one stage amplifier due to the large amplified spontaneous emission (ASE) in the small-signal amplification. The 1040-nm pulse trains are selected from the Ti:Sapphire laser by a dichroic mirror, and are first amplified to the average power of 2.5 mW by a first-stage fiber amplifier. Due to the limited gain bandwidth of the Yb-doped fiber [shown in Fig. 3-2 (b)], the spectrum of the amplified pulses is narrowed to 22 nm after the first stage [shown in Fig. 3-2 (c)]. In the second stage amplifier, the output spectrum is further narrowed to a full-width at half-maximum (FWHM) of 13.8 nm, and the power is amplified up to 140 mW under diode pump of 200 mW.

In order to obtain fs pulses at 1033 nm, a diffraction-grating compressor based on transmission gratings with a grating period of 1250 lines/mm is used to externally compress the amplified laser pulses. For the compressor working at its maximum diffraction efficiency at 1064 nm, the grating pair is placed at 41.7± Littrow angle. Finally, the FWHM duration of the amplified pulse is compressed to 130 fs, which is 32 times smaller than the uncompressed amplified pulse of 4.2 ps [shown in Fig. 3-2 (e) and (f)].
As mentioned above, since the synchronous pulse trains obtained by the FSA are generated from the same oscillator, the cavity-variation induced synchronization instability can be effectively avoided. In the experiment, the timing jitter is measured as low as 0.55 fs.

3.1.2 Master-slave injection configuration for laser synchronization

Master-slave configuration is most wildly used for synchronizing two individual lasers. In this configuration, the master pulses are injected into the salve laser cavity. And the master co-propagates and interacts with the slave pulse inside the slave cavity. The operation of the slave laser is dependent on the master pulse injection due to XPM effect induced by the master laser. Due to the intensity-dependent XPM, master-slave configuration is more favorable to be applied into a fiber laser. Since the small diameter of single mode fiber providing higher light intensities in the fiber core, XPM effect will be largely enhanced inside the fiber cavity to support a robust timing synchronization. As a typical example for the master-salve configuration, Figure 3-3 presents an experiment on synchronizing an Er-doped fiber laser to an Yb-doped laser source (Li el at., 2009).
With the master-slave configuration, the 1030-nm laser light (generated by using fraction spectrum amplifier) is synchronized to 1560-nm pulse train at a repetition rate of ~80 MHz, as schematically illustrated in Fig. 3-3 (a). When the three lasers operated at free-running mode, the longitudinal frequencies of the lasers varied, as shown in Fig. 3-3 (b). However, when the lasers were synchronized, they would oscillate at a same repetition rate or round trip frequency $f=f_1=f_2=f_3$. In this case, the three laser beams could be treat as one beam with a combined spectral distribution. The experimental setup is shown in Fig. 3-3 (c). The 1030-nm pulses are chosen as the master source. As an independent laser, the Er-doped fiber laser can be mode-locked by carefully aligning the quarter- and half-wave plates inside a unidirectional ring cavity to change the nonlinear polarization evolution. One of the collimators is mounted on a translation stage inside the slave laser cavity so that the cavity length can be slightly changed with its repetition rate to match the corresponding master repetition rate. It should be mentioned that the repetition-rate match is a quite important part to realize the passive synchronization. The repetition rate of the Er-doped fiber laser is designed to be 40 MHz, a half of that of master laser. The output pulse is centered at 1560 nm with the pulse width of ~290 fs [Fig. 3-4 (a) and (b)]. As a slave laser under the case of the master pulses injection, the Er-doped fiber laser can be locked at the same repetition rate of the master laser, which is the second harmonic of its own fundamental repetition rate. The radio frequency of the slave laser before and after being synchronized is given in Fig. 3-4 (c) and (d).
Because the two synchronous lasers come from two spatially-separated oscillators in the master-slave configuration, the relative variation of the two cavities limits the synchronization precision to a large extent. Therefore, the relative jitter of the two synchronized lasers is larger than that of the FSA. The integrated timing jitter in the Fig. 3-3 (c) setup is nearly 8.5 fs, which is 15 times larger than that in the FSA experiment.

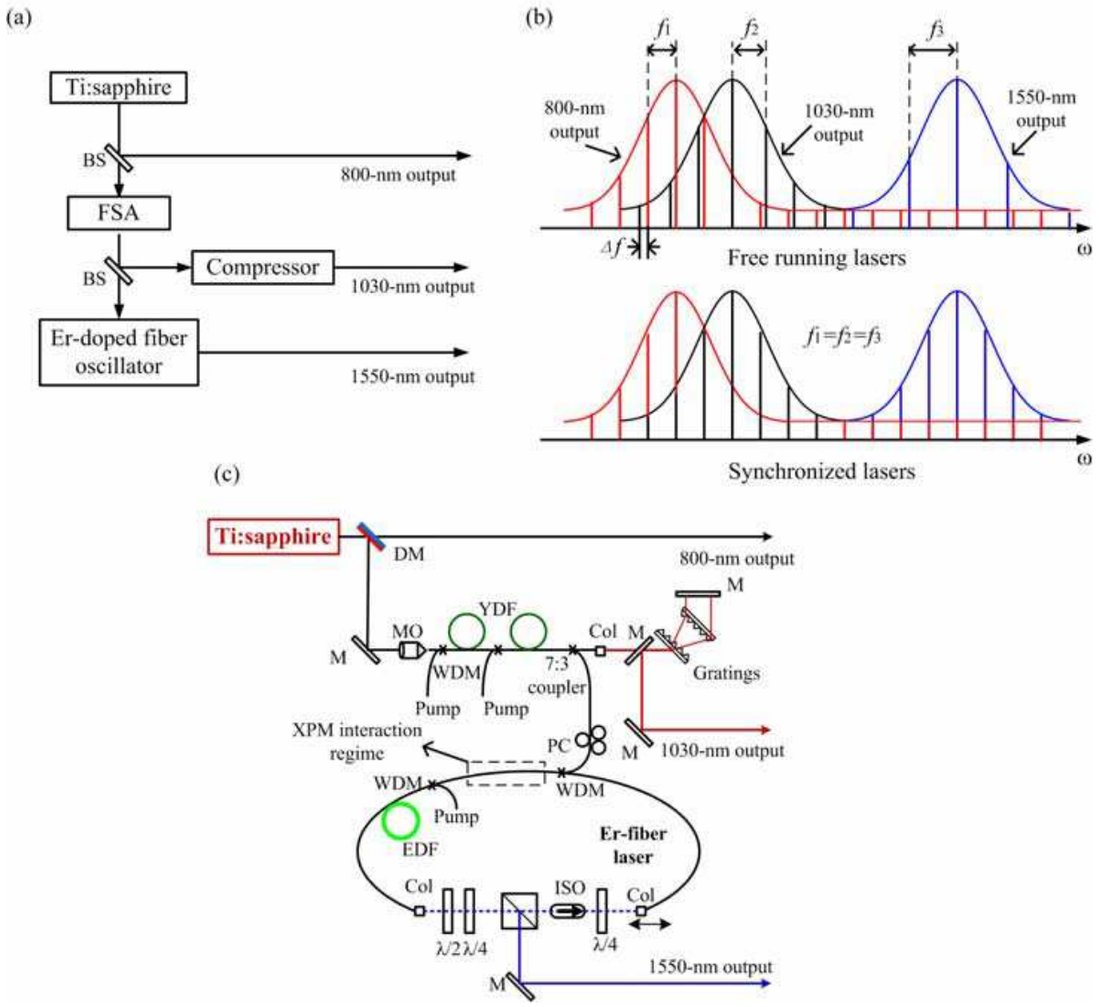

Fig. 3-3. Experimental structure (a), spectral schematic of the synchronized three-color lasers (b) with the experiment setup (c). DM: dichroic mirror (HT at 800 nm and HR at 1030 nm), MO: micro-objective, WDM: wavelength division multiplexing, YDF: ytterbium-doped fiber, EDF: erbium-doped fiber, ISO1: fiber isolator, ISO2: free space isolator, PC: fiber polarization controller, COL: fiber collimator, λ/2 and λ/4: half-wave plate and quarter-wave plate, PBS: polarization beam splitter.

3.1.3 Synchronization achieved by using Kerr nonlinear medium

For fiber lasers, master-slave configuration is considered to be a simple but efficient scheme because single-mode fiber has a very small core diameter to restrict light in a narrow area resulting high light intensity. However, in free space, it is difficult to keep light in a small area for a distance as long as the walk-off length. Thus, to realize a passive synchronization between two solid lasers, Kerr-type nonlinear medium is required to support a strong XPM effect for two synchronous pulses interacting with each other (Apolonski el at., 1993; de Barros & Becker, 1993; Fuerst el at., 1996; Telle el at., 1999; Jones el at., 2000; Apolonski el at., 2000; b Rusu el at., 2004). This is because the Kerr medium can provide large nonlinearity compensating for the disadvantage of low light intensity.

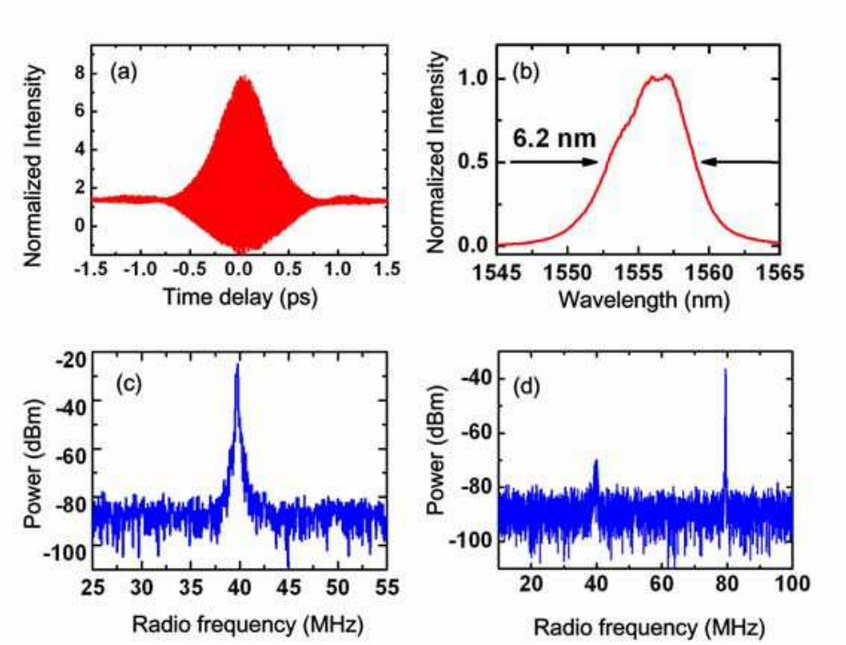

Fig. 3-4. Pulse duration of the synchronized mode-locked EDFL pulses (a) with the corresponding spectrum (b) and the radio frequency spectrum of the mode-locked EDFL pulses before (c) and after (d) synchronization.

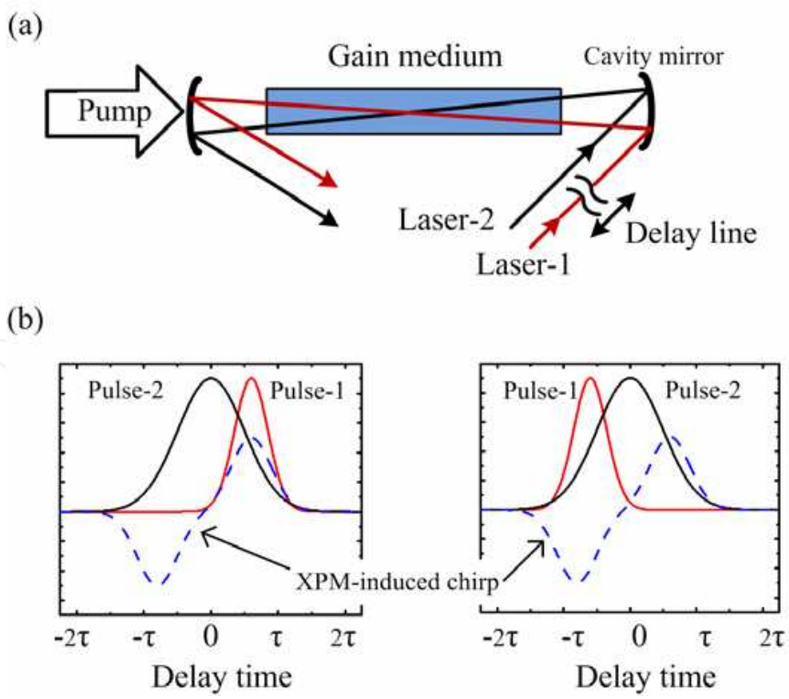

Fig. 3-5. The experimental scheme for synchronization by sharing a same gain medium (a) and the XPM induced frequency chirp for Laser 2 (b). The red line is for laser-1 and black one is for laser-2.

Cavity-shared laser synchronization can be realized by using a setup as shown in Fig. 3-5 (a), where the two lasers share the same gain medium of Ti:sapphire crystal. Due to the broad gain spectrum of the Ti:sapphire crystal, the two lasers can oscillate at different wavelengths. Since the gain medium exhibits Kerr nonlinearity, the two lasers can interact with each other in such a high-nonlinearity medium resulting in a XPM-synchronization as discussed in Section 2.1. In this case, the two lasers are cross-mode-locked at matched cavity-lengths. Once Pulse-1 goes before (behind) Pulse-2 caused by the cavity variation, it will interact with the falling (rising) edge of Pulse-2, as shown in Fig. 3-5 (b). As a result, Pulse-1 obtains a positive (negative) frequency chirp from Pulse-2, which compensates for the cavity variation when Pulse-1 propagating in normal dispersion cavity.

3.2 Mode-locked nanosecond pulse generation and synchronization

Synchronization of ns pulse trains and even precisely phase-locked ns laser arrays are required in many high-energy physics experiments, such as in the development of high-energy laser pulses for particle acceleration, and laser synchronization with x-rays or electron beams from synchrotrons (Schoenlein el at., 1996; Baum & Zewail, 2007). Conventionally, the synchronous ns laser pulses can be obtained by Q-switching technique and active synchronization scheme with a complicated electronic feedback system. In this section, we will introduce a simpler scheme to passively synchronize a mode-locked ns laser with a ps laser by using XPM and peak-power clamping effects.

3.2.1 Peak-power clamping effect

Recently, it is found that Erbium-doped fiber laser with a long cavity can generate ns square mode-locked pulses by the peak-power clamping effect. In order to discuss this effect, a simplified Er-fiber laser scheme is illustrated in Fig. 3-6 (a) with a cavity-length of L.

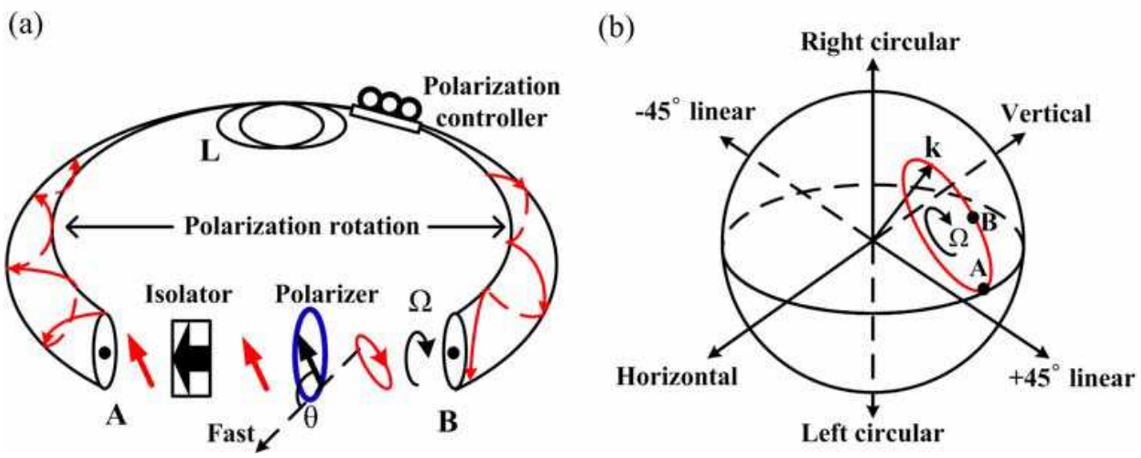

Fig. 3-6. The simplified Er-doped fiber laser cavity (a) and a corresponding poincaré sphere diagram (b).

After passing through the polarization dependent isolator (ISO), the round-trip transmission of the laser pulse can be expressed by (Matsas el at., 1992; b. Li el at., 2009):

$$T_p = \cos^2(\Omega) - \frac{1}{2}\sin(2\theta)\sin[2(\theta-\Omega)]\times[1-\cos(2\pi L / L_{b0})] \tag{7}$$

where Ω is the rotation angle induced by both polarization controllers and fiber intrinsic linear birefringence and θ the azimuth angle of the polarization-dependent isolator with respect to the fast axis. The beat length L_b is power-dependent in a case of light power being high enough to bring in a nonlinear effect. Assuming that the pulse is linearly polarized at $\theta = 45^\circ$, the beat length will be (b. Li el at., 2009):

$$\frac{L_b}{L_{b0}} = \left(\frac{3}{8} + \frac{5}{8}\sqrt{1+p^2}\right)^{-1/2} \tag{8}$$

where L_{b0} is the linear beat length of the birefringent element (in this case, the total power-independent birefringence of the cavity) and the normalized power P is defined as $P = 2n_2 I/3\Delta n$, where I is the light intensity, n_2 is the nonlinear refractive index and Δn is the refractive difference between the two birefringent axes. According to Eq. (8), the requirement for the lowest normalized power that maximizes the round-trip transmission in Eq. (7) can be deduced as:

$$\left(\frac{3}{8} + \frac{5}{8}\sqrt{1+p^2} = \frac{2}{2 + L_{b0}/L}\right. \tag{9}$$

$$P_{sw} = \sqrt{\frac{1}{25}(2(2 + L_{b0}/L)^2 - 3)^2 - 1} \tag{10}$$

The switching power decreases with the fiber length according to Eq. (10). Note that the peak power will be clamped to maintain the condition when the pulse power is sufficient to meet the maximum round-trip transmission. In this situation, without the injection of the master laser, the slave laser could be self mode-locked with the square ns mode-locking mode by adjusting the polarization.

In the situation where a master pulse is injected into the slave laser, the injected pulse induces a nonlinear phase shift of the slave laser between two orthogonal polarization modes as (Agrawal, 2001)

$$\Delta\varphi_{XPM} = \frac{4\pi n_2 |E_p|^2 L_{eff}}{3\lambda} \tag{11}$$

where L_{eff} is the effective interaction length of XPM coupling between the master and slave lasers, E_p the electric field of the injection master laser in the slave laser cavity, and λ the central wavelength of the slave laser. As the XPM-induced nonlinear phase shift is merely related to the power of the master pulse, it just behaves as an equivalent linear polarization rotating element Ω in Eq. (7). As a result, the master laser injection functions as an optical trigger to synchronize the slave laser, while the power for the slave reaching its first maximum round-trip transmission is still maintained. To specifically describe the process of ns pulse generation, an experiment of synchronizing an ns Er-doped fiber laser (slave laser) to a ps Yb-doped fiber laser (master laser) is discussed (b. Li el at., 2009).

In this experiment, a master-slave configuration is employed as shown in Fig. 3-7. The master [Fig. 3-7 (a)] is a passively mode-locked Yb-fiber laser with a repetition rate of 1.91 MHz. The initial pulse width of the master laser is 47 ps centering at 1053 nm. Before being injected into the slave laser, the master laser is at first amplified to 150 mW by an Yb-doped

fiber amplifier. As a slave laser [Fig. 3-7 (b)], an Er-doped fiber laser can be mode-locked at its fundamental repetition rate of 956 kHz, which is half of the master laser's repetition rate, when it is pumped by a 450 mW fiber-pigtailed diode laser at 980 nm. In order to increase the peak-power clamping effect for generating ns pulses, a 200-meter-long single-mode fiber is installed in the slave cavity.

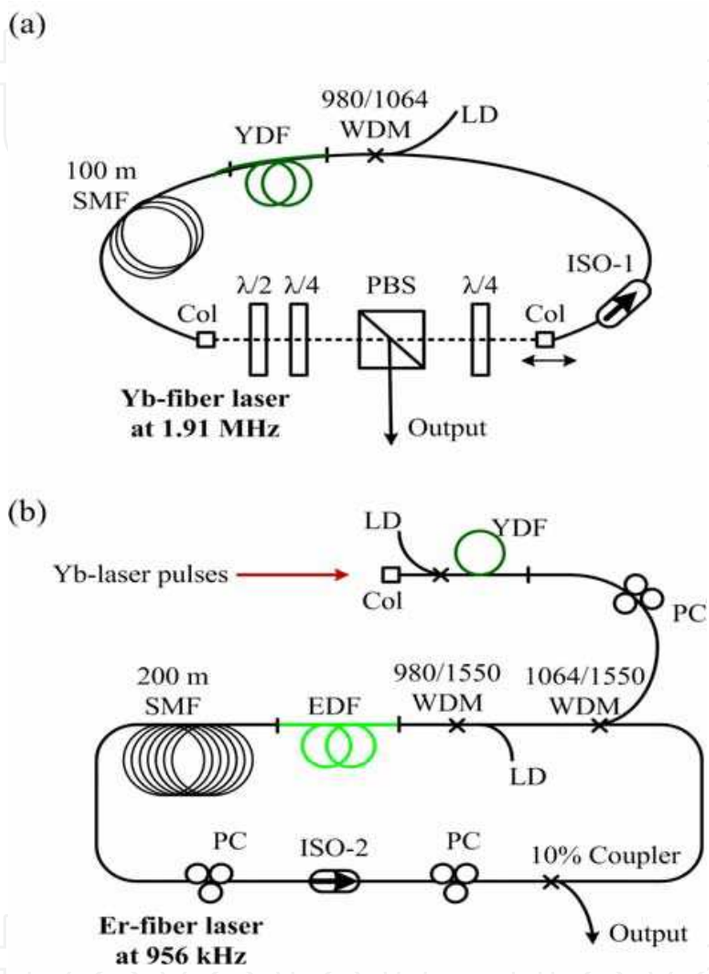

Fig. 3-7. Experimental setup of Yb-doped master fiber laser (a) and Er-doped slave fiber laser (b). YDF: Yb-doped fiber; YDFA: Yb-doped fiber amplifier; EDF: Er-doped fiber; Col: collimator; ISO1 & ISO2: isolators; WDM: wavelength-division multiplexing; PBS: polarization beam splitter; PC: polarization controllers.

Here, we intentionally make the two lasers working at different repetition rates, because the ns fiber laser needs long cavity for offering large peak-power clamping effect while the ps laser requires short one for inducing less dispersion. When the synchronization is achieved between the two lasers, the repetition rate of the slave laser will jump to its second harmonic mode equaling to that of the master laser, while its pulse duration will be reduced to half of the original value according to the peak-power clamping effect, as illustrated in Fig. 3-8. In this experiment, the effects induced by the peak-power clamping in ns-ps synchronization can be summarized as follows.

Firstly, the pump power threshold for the ns pulse generation is inversely proportional to the laser repetition rate. In the experiment, the pump power threshold for the free-running square mode-locking is 200 mW. With the master injection, the Er-laser is synchronized to run at its second harmonic repetition rate due to the XPM-induced nonlinear polarization rotation, and the threshold for the mode-locking is decreased to 50 mW. Meanwhile, with the maximum pump power of 450 mW, the free-running pulse duration is 11 ns as shown in Fig. 3-9 (a), the corresponding spectra is shown in Fig. 3-9 (b). While, the synchronous square ns pulses exhibits a duration of 5.5 ns [Fig. 3-9 (c) with corresponding spectrum at

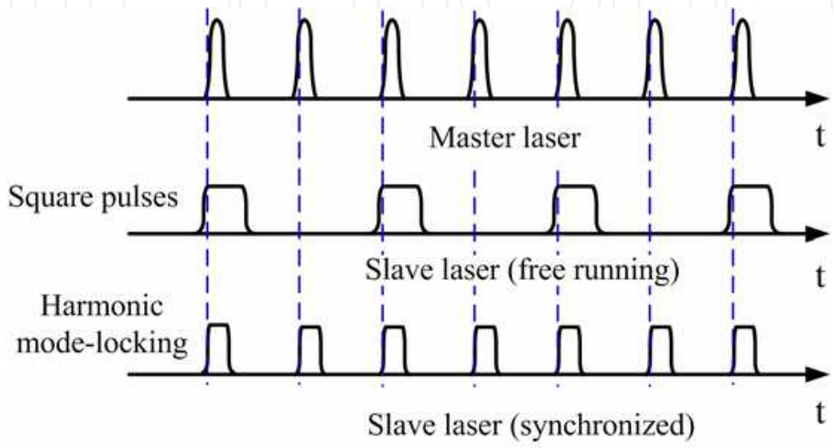

Fig. 3-8. Schematic diagram of laser pulse trains for the ps-ns synchronization experiment.

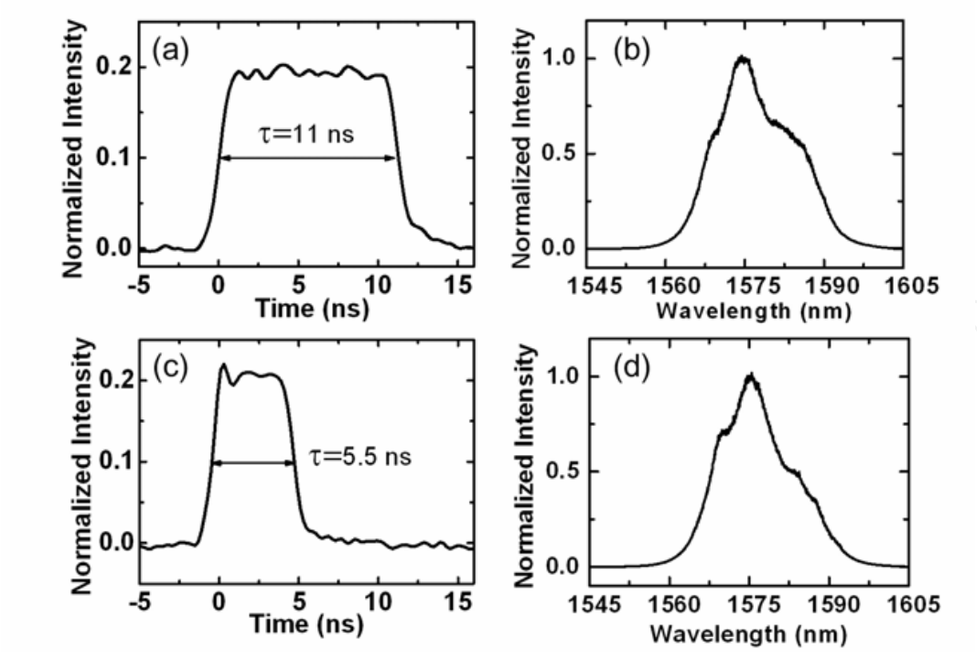

Fig. 3-9. Free-running square mode-locking waveform of the slave Er-laser (a) and its corresponding spectrum (b); Synchronized mode-locking waveform of the slave Er-laser (c) and its corresponding spectrum (d).

Fig. 3-9 (d)] at the pump power of 450 mW, exactly half that of the free-running pulses as an indicative of peak-power clamping at the same level due to the induced switch from the fundamental to the second harmonic mode-locking.

Secondly, the pulse shapes of the synchronously mode-locked Er-laser critically depend on the pump power. As shown in Fig. 3-10, when the pump power is below the threshold value, the output pulse is not a square one because the energy stored in the pulse is not sufficient to sustain the square wave. In this case, the peak power is increased with the pump power. When the pump power reaches the threshold, square mode-locked pulses are generated with an obvious rising of the pulse tail part (Fig. 3-10). As the pump power increases further, the pulse is stretched linearly with the pulse energy due to the peak-power clamping effect.

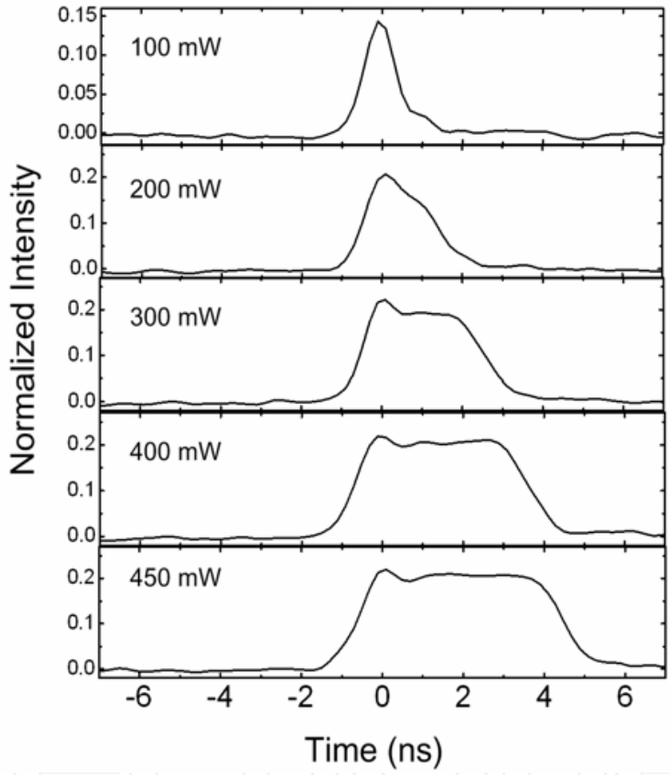

Fig. 3-10. Synchronized pulse trace of the slave Er-doped fiber laser dependent on the pump power.

Thirdly, in the ns operation case, the peak power of slave laser is clamped in a constant value independent on the pump power. As shown in Figs. 3-11 (a) and (b), the output power is almost linearly increased with the pump power, while the peak power maintains around 3.3 W at different pump powers in the square mode-locking state. Since the energy stored in the laser cavity is kept the same at the same pump power but the synchronized pulse repetition rate is doubled, the pulse energy in the free-running state is halved in synchronized mode-locking state and the peak power of each pulse is clamped at the same value. As a result, the pulse duration of synchronous Er-laser is half of that in the free-running state as shown in Fig. 3-9.

Fourthly, the pulse duration of the synchronous slave laser does not change with the injection master laser power. Therefore, in the whole experiment, the peak-power clamping effect is the main reason for square-shaped pulse and the injected master pulse just acts as a trigger to synchronize the square ns mode-locking. As a direct consequence of the peak-power clamping effect, much longer pulse duration can be achieved with higher pump powers.

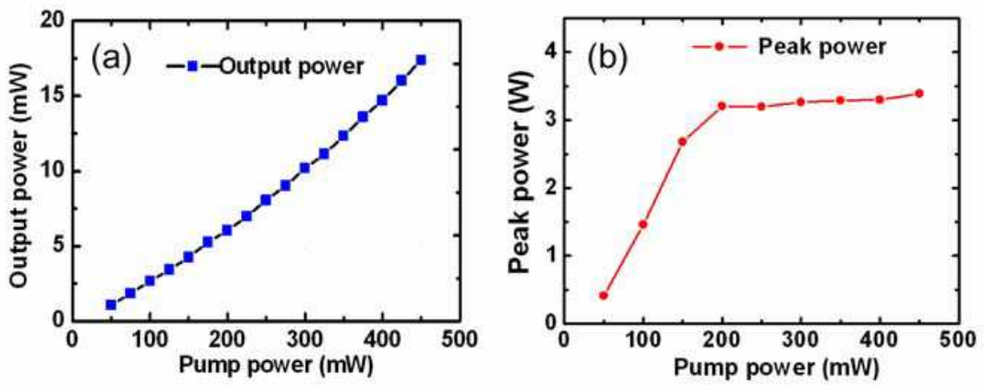

Fig. 3-11. Output power (a) and the peak power (b) of the slave laser as a function of the pump power.

3.2.2 Mismatch tolerance in synchronization

As mentioned before, mismatch tolerance is a crucial index for judging a passive synchronization system. Larger tolerance value means a stronger capability for system standing against variation of cavity length induced by instability of environments. Usually, when a passive synchronization is achieved, the slave laser will run at the same repetition rate with the master laser. In synchronization region, the repetition rate of slave laser is independent with its cavity-length. However, once the cavity-length exceeds the tolerance range, the slave laser will operate in a free-running mode, which means the two lasers are unsynchronized. To measure the mismatch tolerance value, at least one of the two lasers should have a length tunable cavity. The following example will be used to expatiate upon the measurement of mismatch tolerance (Li & Gu el at., 2009).

In the ps-ns synchronization experiment, part of the output pulses from the master and the slave are detected independently in order to monitor the synchronization of the two lasers. The oscilloscope is triggered by the master pulse trains. Only when the synchronization is achieved, the slave pulse trains can be clearly displayed on the oscilloscope. In order to tune the master cavity length, a translation stage with precision of 10 nm is placed inside the master cavity, as shown in Fig. 3-12 (a) (the red dashed box). When the master cavity length mismatch is changed from the −1.3 to 1.3 mm around zero position, the repetition rate of the slave laser keeps the same as the master laser [Fig. 3-12 (b)]. However, beyond the ±1.3 mm range, the slave laser will jump back to its fundamental repetition rate of 956 kHz. In this case, the synchronization is ceased. This maximum mismatch range of 2.6 mm is a quite large value for this system against environmental vibrations in comparison with previous XPM-synchronization experiments (Wei el at., 2002; Yoshitomi el at., 2006).

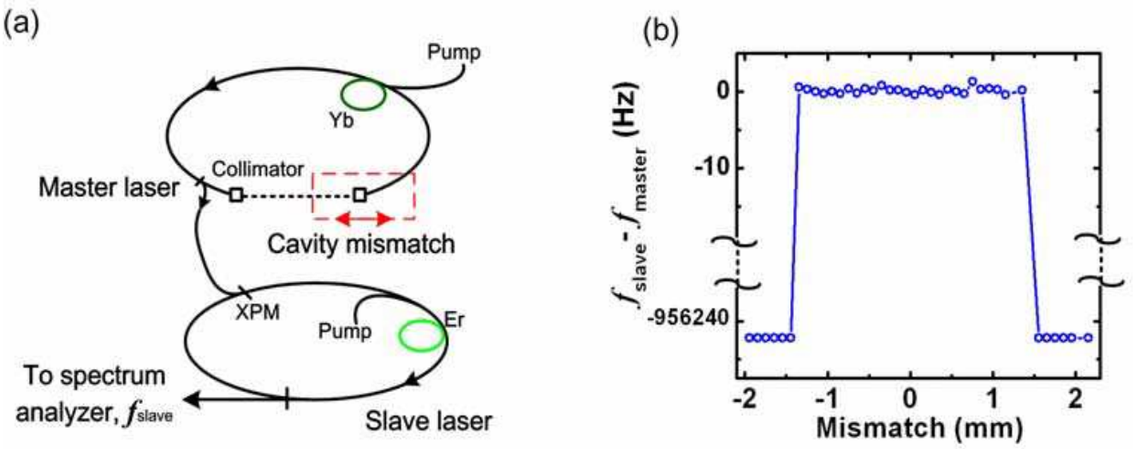

Fig. 3-12. (a) Schematic setup of cavity mismatch measurement and (b) cavity mismatch for the master and slave fiber laser: f_{master} and f_{slave} are the repetition rates of the master and slave lasers, respectively. In the synchronization region, the repetition rate of the slave laser equals to that of the master laser. While beyond that region, the slave laser will jump back to its fundamental repetition rate.

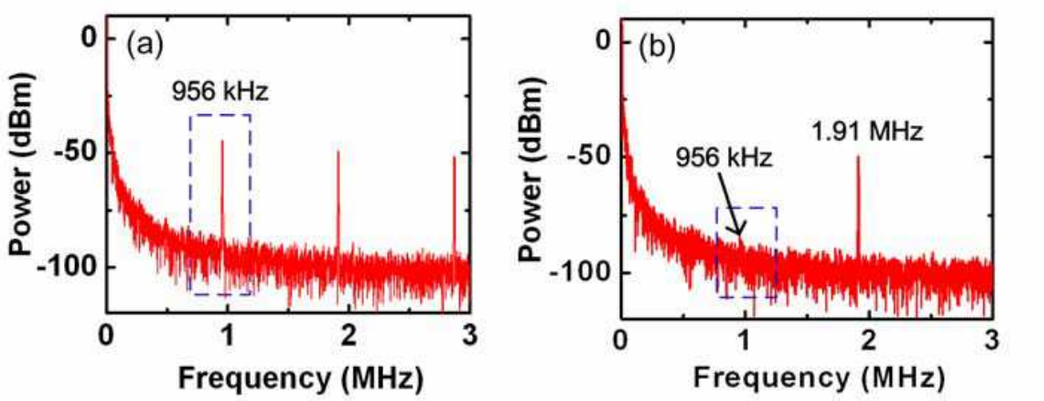

Fig. 3-13. (a) RF spectrum of the free-running repetition rate and (b) synchronous repetition rate.

To further monitor the synchronization state, the output signal of the slave Er-fiber laser is inputted into a spectrum analyzer with a resolution of 1 Hz as the master cavity length is tuned. In the free-running regime, the slave laser oscillates at its fundamental repetition rate of ~956 kHz [Fig. 3-13 (a)]. While in the synchronization regime, the fundamental repetition rate of the slave laser is fully restrained (at least 50 dB) and only its harmonic signal can be seen as shown in Fig. 3-13 (b).

3.2.3 The measurement of timing jitter

Usually, jitter is a concept in the fields like electronics and telecommunications to evaluate the time variation of a periodic signal in relation to a reference clock source. As in frequency domain, the concept of jitter is represented as "phase noise" caused by temporal instabilities. The concept of jitter or timing jitter has been extended to explain the relative

time fluctuation between two synchronous optical pulses. Until now, many methods have been reported to measure the timing jitter for synchronous lasers. As a widely-used method for timing jitter measurement, optical cross correlation technique is employed to indirectly measure the ultra-fast timing jitter (Paschotta, 2004; Foreman el at., 2007; Chen el at., 2006). The theory and practical details of such kind of jitter measurement is discussed with an example based on the FSA synchronization experiment (Li el at., 2009). The experimental setup is shown in Fig. 3-14 (a). In general, the cross-correlation based timing jitter measurement is designed to linearly connect the time fluctuation, $\Delta\tau$, on the order of femtosecond between the two synchronous pulses with the intensity fluctuation, Δi, of the sum frequency signal, as shown in Fig. 3-14 (b). This is because the time fluctuation in fs region is usually too fast to be directly measured by lots of electronic equipments. However, with cross-correlation technique, the fast time variation can be reflected by the measurable intensity changes of the sum frequency signal and then be recorded by a spectrum analyzer for calculating the exact value of the time fluctuation (timing jitter).

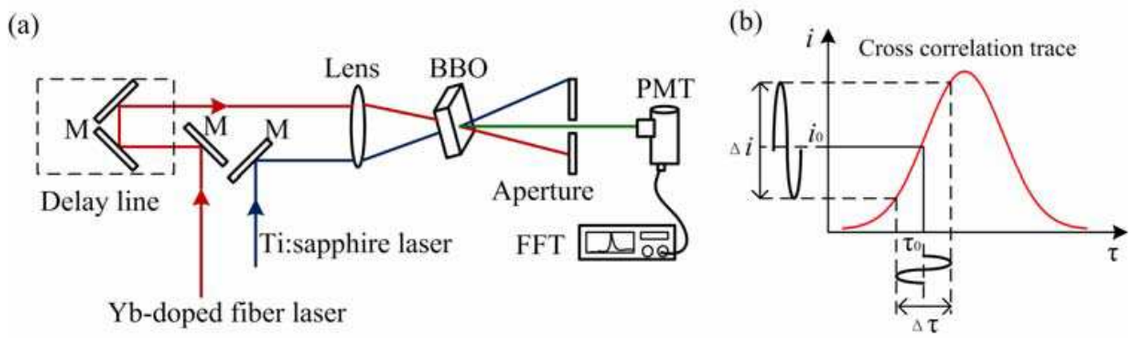

Fig. 3-14. Experiment layout (a) and schematic diagram of the timing jitter measurement with optical cross correlation. M: mirror; BBO: β-barium borate crystal; FFT: fast Fourier transformed spectrum analyzer; PMT: photomultiplier tube.

In the measurement, the Yb-doped fiber laser beam (1030 nm) is crossed with a part of the rest of Ti: sapphire laser beam (800 nm) in a 0.5-mm β-barium borate (BBO) crystal to generate the sum frequency signal at ~452 nm. The Ti: sapphire laser beam passes through a time-delay line. When the delay is scanned, the SFG is detected by a photomultiplier tube (PMT, 10-KHz bandwidth) and the cross-correlation trace between the two fs pulses is recorded and shown in Fig. 3-15 (a).

In order to obtain the jitter power spectral density and its integrated RMS timing jitter, the time delay of the two pulses is positioned at the half-maximum of the cross-correlation signal where the signal can change linearly with the delay time. The Fourier-transformed spectrum of the fluctuation of the correlation intensity is recorded by an FFT spectrum analyzer (SRS, SR760), as shown in Fig. 3-15 (c).

The noise level is normalized against carrier power and bandwidth resolution and expressed in units of dBc/Hz$^{1/2}$. The contribution of timing jitter comes mainly from the band within 1~10 kHz. The noise sidebands are related to amplitude noise and timing jitter by (Chen el at., 1996; Wilcox el at., 2006):

$$S_n(f) = S_E(f) + (2\pi n f_0) S_{JE}(f) + (2\pi n f_0)^2 S_J(f)\,, \tag{12}$$

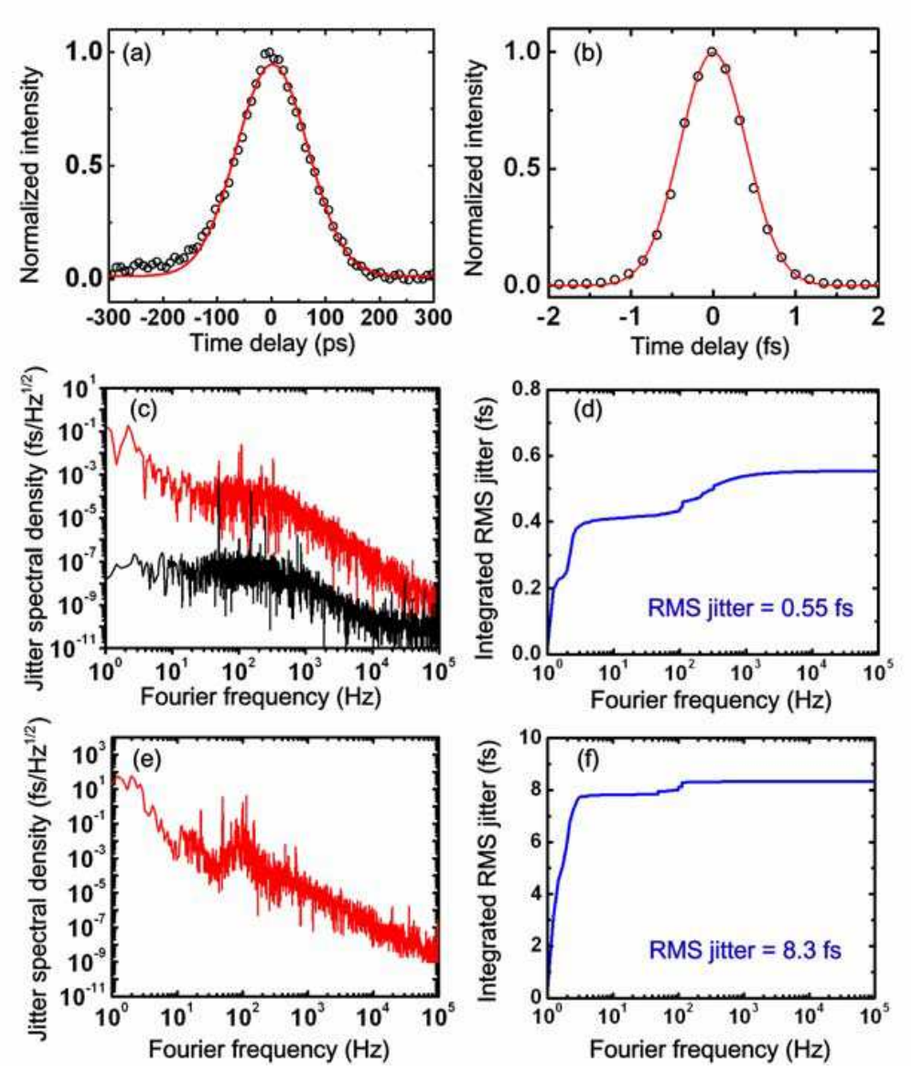

Fig. 3-15. Cross-correlation trace of the synchronized 800-nm and 1030-nm laser pulses (a) and for 1030-nm and 1550-nm pulses (b); relative jitter spectral density (c) and integrated RMS timing jitter (d) of the synchronized 800-nm and 1030-nm laser pulses, while the jitter spectral density of the background noise was shown in gray; the jitter spectra density (e) and the corresponding timing jitter (f) for 1030-nm and 1550-nm synchronization.

where $S_n(f)$ is the sideband noise spectral density function, $S_E(f)$ is the pulse energy noise spectral density function, $S_{JE}(f)$ is the timing-to-amplitude noise coupling spectral density, $S_J(f)$ is the jitter spectral density function, f is the carrier offset frequency, f_0 is the cavity repetition rate, and n is the harmonic number. The experimentally measured sidebands are integrated over the measurement bandwidth, yielding the quantity:

$$\int_{f_1}^{f_2} S_n(f)df = \frac{\sigma_E^2}{2} + (2\pi n f_0)\frac{C_{JE}}{2} + (2\pi n f_0)^2 \frac{\sigma_J^2}{2}, \tag{13}$$

where f_1 and f_2 are the start value and end value for integration, respectively, σ^2_n is the total noise power, σ_E is the RMS normalized pulse energy fluctuation, σ_J is the total timing jitter

and C_{JE} is the cross-correlation term between pulse timing jitter and normalized pulse energy fluctuation. The factor of 2 is for the single sideband noise. For the sake of simplicity, we merely consider the contribution from the term of timing jitter at the fundamental mode of *n=0*, and then transform the spectral density to the time-related one by (Jiang el at., 2002; Haus & Mecozzi, 1993; Hönninger el at., 1999; Eliyahu el at., 1997):

$$T(f) = \frac{S(f)}{2\pi f_0} \text{ (s/Hz}^{1/2}\text{)}. \tag{14}$$

Thus, the RMS timing jitter σ_{RMS} can be calculated by:

$$\sigma_{rms} = \sqrt{\int_{f_1}^{f_2} [T(f)]^2 df} \text{ (s)} . \tag{15}$$

By this way, the timing jitter between the 800-nm pulses and the 1030-nm pulses is calculated to be 0.55 fs, as shown in Fig. 3-15 (d), according to the integration from 1 Hz to 100 kHz. Meanwhile, with the same method, the cross-correlation trace and timing jitter are also measured for the 1030-nm pulses and 1550-nm pulses obtained in section 3.1.2 as shown in Figs. 3-15 (b) and (e), respectively. The jitter between the 1030-nm and 1550-nm lasers is nearly 8.3 fs [Figs. 3-15 (f)]. Actually, for achieving a three-color laser source, one can easily use fraction spectra amplification technique to obtain synchronous pulse trains at 800 nm and 1030 nm, and then synchronize the 1030-nm pulses to 1550-nm laser by utilizing the master-slave configuration for fiber lasers.

3.3 XAM-based synchronization scheme

Up to now, all the passive synchronization schemes discussed above are applicable to ultrashort mode-locked lasers at repetition rate higher than MHz, but inapplicable to mode-locked ns-duration lasers generated at sub-MHz repetition rate. The importance of such synchronous ns pulses has been discussed in the introduction part of this review chapter. Because the sub-MHz ns pulses are conventionally obtained by Q-switching technique, the corresponding synchronization employs active methods. However, the combination of Q-switching and active synchronization has to share same electronic triggers with a quite large timing jitter as limited by the electronic circuits. Even the ns pulses can be achieved in a fiber laser with a long ring cavity, the XPM in the fiber is still limited by the walk-off length and high peak power required to induce sufficient nonlinearity for a tight synchronization. Efficient all-optical techniques are desired to precisely synchronize sub-MHz laser pulse trains.

Recently, a synchronization scheme of XAM was found to permit synchronization at low repetition rates with large tolerable cavity-length mismatches (a. Yan el at., 2009). Compared to XPM-based synchronization, XAM relaxes the restrictions on peak powers of interacting pulses. In the XAM-based synchronization scheme, the master-slave modulation effect is largely enhanced by using a resonant absorption medium in the slave cavity. Thus, synchronization can be achieved in a 800-m-long fiber laser with a repetition rate of ~250 kHz. We will present here an experimental example of XAM-based synchronization for individual lasers at low repetition rates. The XAM triggers synchronous square ns mode-locking sensitive to the injected master laser power, which is unique for the XAM-based synchronization and differs from the XPM-based synchronization as discussed in the previous sections.

3.3.1 Synchronization between Sub-MHz femtosecond and nanosecond lasers

In general, XAM is very weak in non-resonant media, while it becomes comparable to or even larger than XPM in near-resonant media. As an example, we present XAM-based synchronization for low-repetition-rate lasers in the master-slave configuration as schematically shown in Fig. 3-14. A tight synchronization between a 250-kHz Ti:sapphire laser (TiS) and an ns Yb-doped fiber laser is achieved by using enhanced-XAM in an Er-doped fiber inside the Yb-doped fiber laser cavity. In the Er-fiber, the TiS pulse at 800 nm behaves as pump as well as controlling pulse (optical trigger) causing a transition of Er^{3+} from energy level $4I_{15/2}$ to $4I_{9/2}$. In the absence of the trigger pulse, Er^{3+} ions will drop back to and then stay at the level $4I_{15/2}$ through spontaneous emission. The trigger-induced transitions between the energy levels introduce a periodical modulation for the refractive index in the Er-fiber, resulting in the robust synchronization between the trigger pulse and the slaved pulse.

How does the XAM induce a feedback mechanism in the synchronization system? In fact, as the resonant media at 800 nm, the Er- fiber absorbs the TiS pulses with a corresponding refractive index change, resulting in a XAM-induced nonlinear polarization rotation (NPR) for the co-propagating Yb-fiber laser pulses. For the slave pulse, pulse spectral shift accompanying with XAM-induced NPR compensates for the fiber cavity variations to keep the robust synchronization. The details of the theory for XAM applying in synchronization are still under investigation.

As schematically shown in Fig. 3-16 (a), a mode-locked TiS laser (RegA 9000 from coherent Inc.) operates as a master laser to deliver a 250-KHz, 70-fs pulse train. Its spectrum width is ~60 nm with a center wavelength of 800 nm. The salve laser is an Yb-doped fiber oscillator pumped by a 976-nm, 300-mW diode laser. The center wavelength of the salve is at 1041 nm with pulse power of ~3-mW. To oscillate at the same repetition rate with the master, the fiber laser stretched its cavity with ~800 m of single-mode fiber. Besides, the fiber cavity includes 1.5-m-long Yb-doped fiber as the gain medium and 1-m-long Er-doped fiber (unsaturated absorption at 800 nm, ~3.0 dB/m; dopant concentration, 5.4×10^{24} m^{-3}) for inducing enhanced XAM. Without synchronization, the fiber laser pulse duration can be tuned from sub-ns to ~10 ns roughly by adjusting two sets of polarization controllers and accurately by rotating a half-wave plate placed between the two collimators.

In order to induce XAM into the fiber laser, a portion of ~200 mW of the TiS laser is used and nearly 20 mW is injected into a 0.5-m-lomg single-mode fiber with a microscope objective (×40). The injected pulse is further coupled into the fiber laser cavity through 800/1064-nm wavelength-division multiplexer (WDM) immediately followed by the 1-m-long Er-doped fiber. Through the 800/1064-nm WDM only 10-mW mater power is left. After the injection, the synchronous pulses can be obtained by carefully adjusting the polarization controllers inside the fiber cavity. Finally, timing jitter of ~0.6 fs is achieved and the cavity mismatch tolerance is extended to 8.2 cm, which is the largest value ever recorded in passive experiments, due to the long cavity and absorption effect. During cavity mismatch measurement, it is also found that the ns Yb-doped fiber laser can keep the synchronization state by shifting the center wavelength from 1038 nm to 1043 nm.

Usually, there are three keys important for the XAM synchronization. First, for a fiber laser with hundreds-meters-long fiber cavity, the fiber laser pulse must be highly chirped due to the dispersion effect inside the cavity. Considering the normal dispersion for the near-infrared laser light, the slave pulse will propagate with red head and blue tail. Secondly, the master laser at 800 nm is able to excite Er3+ from energy level $I_{15/2}$ to level $I_{9/2}$ [shown in

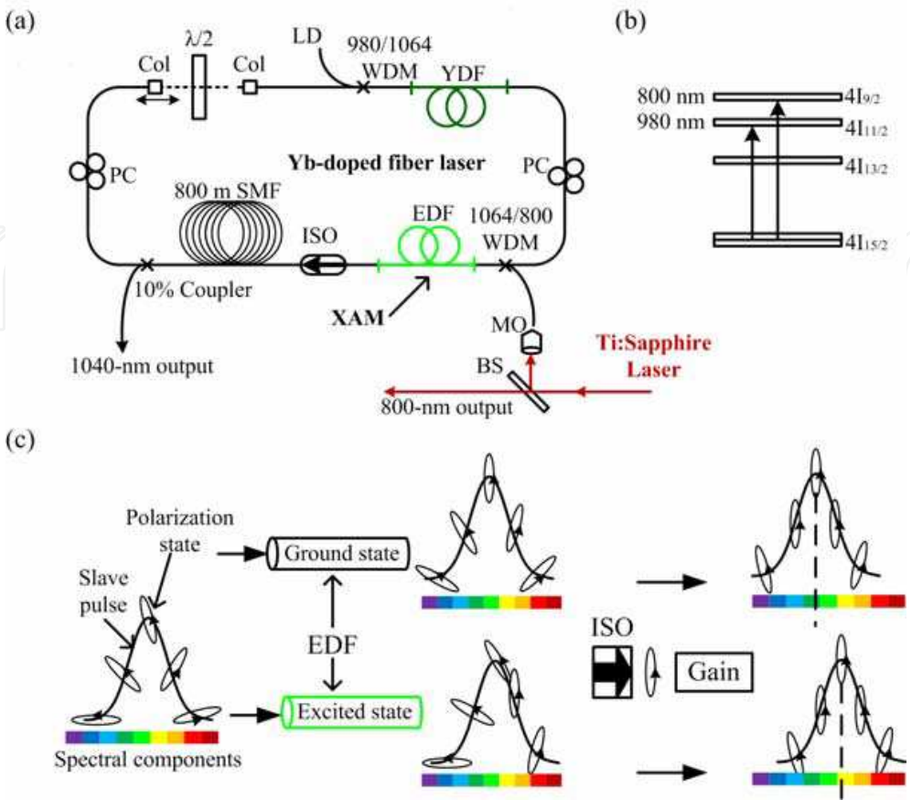

Fig. 3-16. Experimental setup of XAM-based synchronization (a), energy structure of Er-doped fiber (b) and the principle schematic of the XAM synchronization. BS, beam splitter; Col, collimator; OC, output coupler; MO, micro-objective; WDM, wavelength division multiplexer; PC, polarization controller; ISO, Isolator; λ/2, half-wave plate. In (c), when the slave pulse passes through an excited Er-doped fiber, its polarization states will be changed comparing to going through the ground-state Er-fiber. And under the cooperation of the polarization-dependent isolator and the gain medium, the spectral center of the polarization-rotated slave pulse is shifted. Note that this spectral shift is crucial for compensating for relative variation of the repetition rates in the XAM synchronization.

Fig. 3-16 (b)], which changes the birefringence index of the Er-doped fiber. As a result, the polarization state of the co-propagating slave pulse will be changed as illustrated in Fig. 3-16 (c). Thirdly, the polarization-dependent isolator inside the fiber cavity only permits certainly polarized light pass through with a minimum loss. The light with other polarization states will be isolated. The certain polarization state can be achieved by adjusting the polarization controllers inside the fiber cavity, when the salve laser is synchronized. Since the fiber laser cavity is sensitive to environmental fluctuations, the slave pulse will go ahead or behind of the master pulse in the Er-doped fiber. If the slave pulse go ahead of the master pulse, the blue tail of the slave pulse which overlaps with the master pulse will be affected by XAM effect with a polarization rotation so that the blue part could maximally transmit the isolator and be amplified by the Yb-doped gain fiber while the red part is isolated. As a result, the center wavelength of the slave laser is blue shifted, which means in the fiber cavity of normal dispersion the slave pulse is slowed down to match the master pulse in the time

domain. While, if the slave pulse falls behind of the master pulse, a spectral red-shift will be induced to the salve laser for catching up with the master pulse. In the XAM experiment, total spectral shifts of ~3 nm were found to balance with the cavity-mismatch of ~8.2 cm.

3.3.2 Sensitivity of slaved laser to injection power of master laser

In the XAM-based synchronization experiment, the pulse duration of the slave fiber laser can be affected by the injection pulse power of master laser, which is different with the case in the XPM-based synchronization experiment (Section 3.2.1). In the XPM experiment, the master injection influence very little to the ps-ns synchronization realized by peak-power clamping effect, while the injection power plays an important role in the XAM experiment to affect the slave pulse. Thus, to study this sensitivity is helpful for people understanding the mechanism of XAM applied in synchronization experiment.

As we know, in a fiber laser mode-locked by nonlinear polarization rotation (Fermann el at., 1997), the pulse duration is related with the intra-cavity pulse polarization. In the XAM-triggered synchronous square ns mode-locking experiment, when the Yb-doped fiber laser oscillates in the ns regime, the polarization-related pulse duration and its changes can be easily observed on the oscilloscope with a fast photo-detector.

Interestingly, the fiber laser pulse duration recorded on the oscilloscope is highly sensitive to the coupled power (as shown in Fig. 3-15). This sensitivity indicates that the injected master laser behaves as a power-dependent polarization controller by changing the refractive index of the resonant medium through the XAM process. The polarization at different injection power is estimated by comparing its pulse duration with the case of rotating the half-wave plate at a fixed injection power of 7.4 mW. And then the rotation angle is fixed at 326° of the half-wave plate while the master injection power is changed. As a result, it is found that the injected power of 1.8, 3.4, 6.3 and 7.4 mW correspond to the polarization angle of 339°, 335°, 330° and 326°, respectively. These angles are directly read from the half-wave plate. With these angles, we can simply estimated the XAM induced refractive index change $\Delta n(\lambda)$ at wavelength of λ by (Fekete el at., 2009):

$$\Delta n(\lambda) = \frac{\lambda}{\pi L_{Er}} \Delta\theta \tag{16}$$

where θ is the polarization angle, $\Delta\theta$ means the changes of polarization angle which is twice of the change of rotation angle of half-wavelength plate and L_{Er} is the length of the 1-m Er-doped fiber. Therefore, the corresponding change of the refractive index is measured to be nearly -7.5×10^{-8} as the injection power is changed from 1.8 mW to 7.4 mW. Note that 1.8 mW is the lowest injection power for starting the ns synchronization.

Until now, we merely introduce the basic concept of XAM and its phenomenon in the synchronization experiment. The intrinsic mechanism and full theory for the XAM-based synchronization require further exploration. With XAM, we successfully realize the ns laser source synchronized with an fs laser. By amplifying this ns source, we can obtain high-energy synchronous laser sources at sub-MHz repetition rates.

3.3.3 Generation of high-power synchronous laser source

In previous sections, we discuss the realization of different synchronization schemes. Considering many physics researches relaying on the high-power synchronous light source, we focus here on the amplification of the laser light.

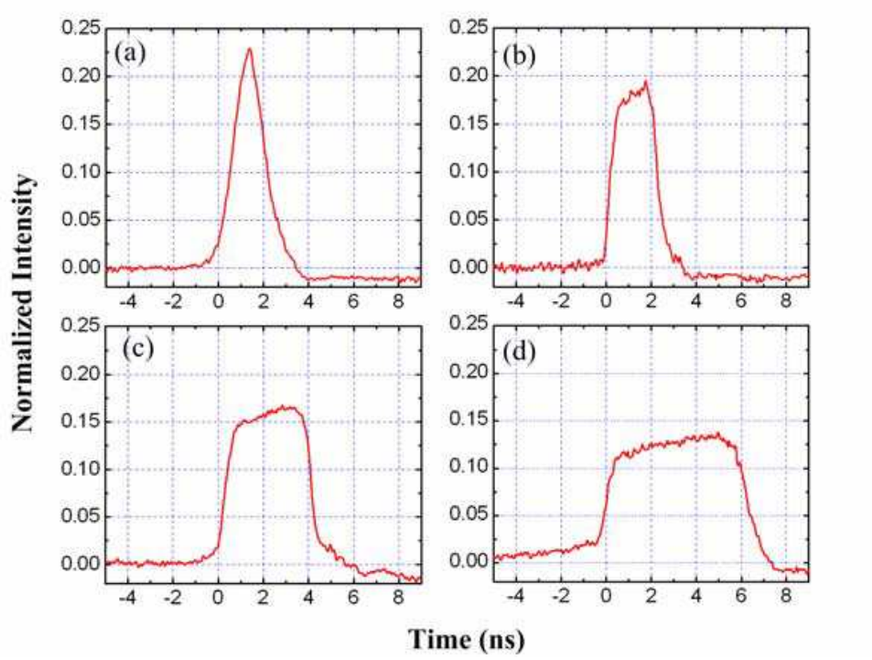

Fig. 3-17. The XAM-induced slave laser sensitivity to the master injection powers of (a) 1.9 mW, (b) 4.4 mW, (c) 6.1 mW and (d) 8.3 mW. The pulses are detected by a 3-GHz photo-detector and recorded by a oscilloscope with bandwidth of 6 GHz.

Recent progress in fiber lasers opens up a new way for high-power laser oscillators and amplifiers. The advent of double-clad fiber technology benefits high-power lasers and amplifiers from kHz to GHz repetition rate (Hao el at., 2007; Papadopoulos el at., 2007). The special fabrication of double-clad fiber not only provides an effective way to transfer the energy from diode lasers into fiber core where the signal pulses propagate, but also ensures diffraction-limited beam quality (a. Limpert el at., 2003). The long signal-pump laser interaction distance can afford a high optical-to-optical efficiency, while the large surface-to-volume ratio results in excellent heat dissipation (b. Limpert el at., 2003). Moreover, large-mode-area (LMA) photonics-crystal double-clad fiber upgrades the threshold of nonlinear effects such as stimulated Raman and Brillouin scattering, while its inner core provides a single-mode operation during amplification (c. Limpert el at., 2003). Therefore, it is a natural idea to combine the temporal synchronization of multi-color lasers with the LMA double-clad fiber amplification technology to attain high-power synchronous lasers.

However, to design a well-performed amplification system, many factors should be taken into account. First, the amplified pulses will suffer from the spectral and temporal distortion, nonlinear phase shifts and nonlinear polarization evolution during the amplification. Especially, some undesirable optical nonlinearity may occur with serious nonlinear phase shifts, since the amplifying laser is tightly guided in the inner cores of the double-clad fibers. Secondly, amplified spontaneous emission (ASE) noises may degrade the synchronization accuracy by inducing detrimental influence into the timing jitter. Thus, in further amplification, special care should be taken to make the seed light having sufficient pulse energy dominating over ASE noises. For this reason, multi-stage amplifiers in cascade can be employed to reduce ASE.

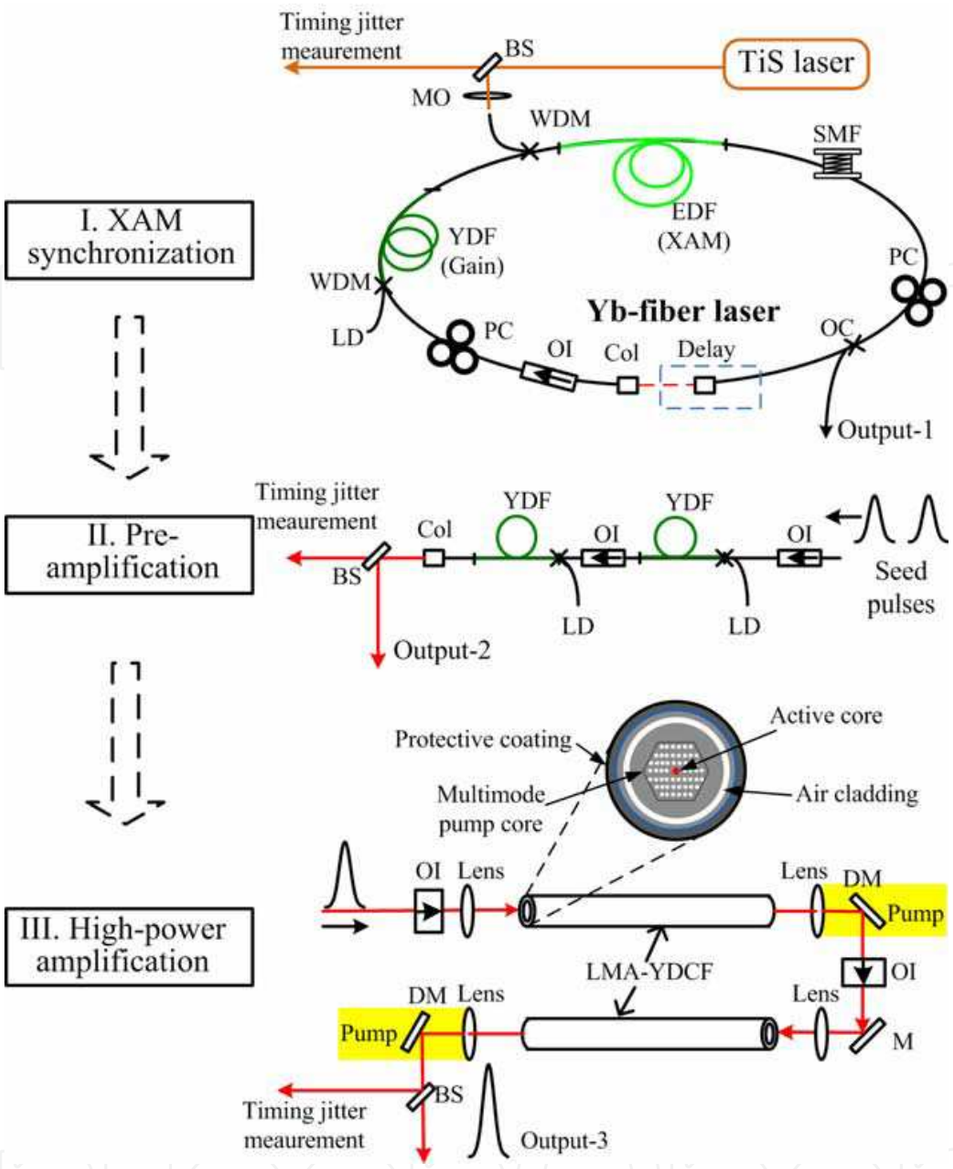

Fig. 3-18. Experimental setup of high-power synchronous ns laser source. BS: beam splitter; MO: micro-objective (×40); WDM: wavelength division multiplexing (980/1041 nm); YDFA: ytterbium-doped fiber amplifier; EDF: erbium-doped fiber; YDF: ytterbium-doped fiber; SMF: single mode fiber; Col: collimator at 1041 nm; OC: 10% output coupler; PC: polarization controller; OI: optical isolator; LD: laser diode ; LMA-YDCF: large mode area Ytterbium-doped crystal fiber; PMT: photomultiplier, FFT: fast Fourier transformed spectrum analyzer.

Previously, based on the XAM-scheme, we achieved a synchronous ns pulse train at repetition rate of 250 kHz. In the following example, the obtained ns pulse is amplified to 131 W (0.55 *mJ per pulse*) by a four-stage amplification system. Meanwhile, the influence of the amplification system on the seed light properties and timing jitter will be studied (b. Yan el at., 2009).

The experimental setup is shown in Fig. 3-18. The ns fiber laser is first synchronized to the TiS laser, and then injected into a multi-stage amplification system which includes a two-stage Yb-doped fiber pre-amplifier and a two-stage LMA-YDCF power amplifier in cascade. In the pre-amplifier, ytterbium-doped single-mode fiber (YbDF350, OFS) of 0.6 m and 1.5 m are used for the first and second stages, respectively, both are pumped by diode lasers at 976 nm. After the pre-amplifier, the fiber laser is amplified to 180 mW. For the first-stage power amplifier, a 1.5-m-long LMA Yb-doped double-clad photonic-crystal fiber is used as a gain medium. Its pump absorption is 10 dB/m at 976 nm with an active core diameter of 40 μm (NA=0.03) and an inner cladding diameter of 200 μm (NA=0.55). The second-stage power amplifier employs 0.85 m-long Yb-doped rod-type photonic-crystal fibers, of which the pump absorption is 30 dB/m at 976 nm, with an active core diameter of 70 μm (NA=0.02) and an inner cladding diameter of 200 μm (NA=0.6). In order to suppress parasitic lasing, the LMA-YDCF ends are sealed to protect the capillaries from environmental influences and polished at an angle of 8°. For the high-power amplifiers, 75% of pump energy is coupled into the inner clad and 60% of the seed power is coupled into the fiber core. With the first-stage power amplifier, the fiber laser pulses are amplified to 4 W, and then are finally boosted to 131 W by the second-stage power amplifier. The slope efficiency of the last amplifier is measured to be 49.5%.

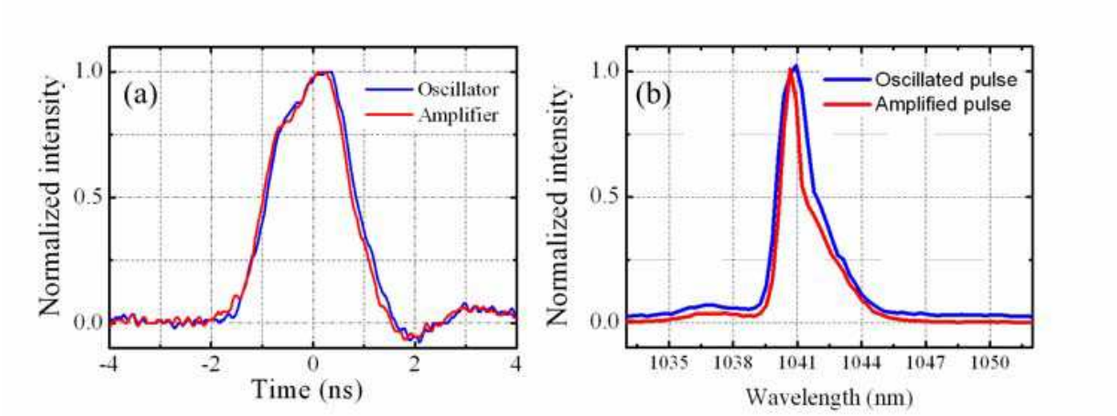

Fig. 3-19. The measured temporal profiles of the synchronized seed fiber laser and the amplified pulses (a) and their corresponding spectra (b).

The corresponding single pulse energy is about 0.55 mJ. This is to the best of our knowledge the highest single-pulse energy for passively synchronized ns lasers. In addition, since the ns light is narrow-band operated, the amplification system brings no obvious spectral variation and temporal distortion into the ns seed pulse, as depicted in Fig. 3-19.

In order to investigate the impacts on the synchronization precision from the power amplification system, the timing jitters between the fs laser pulses and the ns fiber laser pulses before and after the amplification system are measured by virtue of optical cross correlation technique discussed in Section 3.2.3. The Fourier-transformed spectrum of the fluctuation of the correlation intensity is shown by the blue line in Fig. 3-20 (a) with a RMS jitter of about 0.8 ps. The timing jitter between the Ti: sapphire laser beam and the ns fiber

laser beam after the last high-power amplifier approximated 13 ps, as shown in Fig. 3-20 (b). Note that at least two main reasons are responsible for the increase of RMS jitter. Firstly, the two-stage LMA amplifier with a complicated water chilling system is individually placed at an optical table spatially apart from the pre-amplifier and the synchronization system. It is quite possible for the spatial disjunction increasing environmental disturbances (air variation, temperature fluctuation, etc.) to the amplified pulses. Secondly, the pump power fluctuations of the whole four-stage amplifier contribute the RMS jitter augment. It should also mention that the spike in Fig. 3-18 (a), the red line, is mainly caused by the fluctuation of fiber-based amplification system at a frequency of several Hz. Fortunately, compared with the pulse duration as large as several ns, the 13-ps RMS jitter is small enough not to threaten the applications of the high-energy synchronized ns pulses.

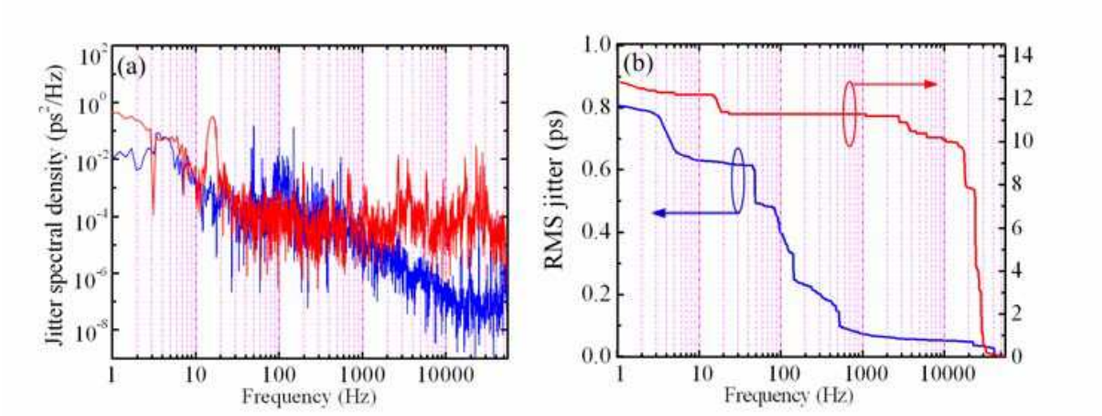

Fig. 3-20. Power spectral density of the jitter (a) for Ti: sapphire laser and ns fiber laser before (blue line) and after (red line) high-power amplifiers and their corresponding integrated RMS jitter from 50 KHz to 1 Hz (b). The narrow peaks in the (a) were due to the 50-Hz electro-disturbance.

4. Conclusion

In this review chapter, passive synchronization between independently mode-locked lasers is introduced with nonlinear effects of XPM and XAM. The mechanism of laser synchronization is mainly due to the reliability of its feed-back system. In the XPM-synchronization, the feed-back system is provided by XPM in coupled-cavity lasers sharing the same Kerr-type nonlinear medium, or independently mode-locked lasers in the configuration with master injection into the slave laser, to compensate the cavity length mismatch. In the XAM-synchronization, the feed-back is realized in a resonant medium for the master laser modulating the medium at different electronic states and indirectly changing the co-propagating slave laser. As the most popular synchronization method, XPM scheme is widely used for ultra-fast lasers with timing jitter as small as several fs, or even hundreds of as. Besides, since it is found that fiber laser with long ring cavity can directly produce mode-locked ns laser pulses, the combination between the long-cavity fiber laser and passive synchronization methods can be used to generate synchronous ns laser pulses which have a lot of applications in physical researches.

5. References

a. Agrawal, G. P. *Nonlinear Fiber Optics* (Academic, New York, 1989), pp. 199–206.

b. Agrawal, G. P.; Badeck P. L. & Alfano, R. R. (1989). *Phys. Rev. B* 40, 5060-5072.

Agrawal, G. P. *Applications of Nonlinear Fiber Optics* (Academic, New York, 2001).

Apolonski, A.; Poppe, A.; Tempea, G.; Spielmann, C.; Udem, T.; Holzwarth, R.; Hänsch, T. W. & Krausz, F. (2000). *Phys. Rev. Lett.* 85, 740–743.

Baldeck, P. L.; Alfano, R. R. & Agrawal, G. P. (1988). *Appl. Phys. Lett.* 52, 1939–1941.

Bandrauk, A.D.; Chelkowski, S. & Goudreau S. (2005). *Journal of Modern Optics* 52 (2), 411-428.

Bartels, A.; Diddams, S.A.; Ramond, T.M. & Hollberg, L. (2003). *Opt. Lett.* 28, 663–665.

Bartels, A.; Newbury, N. R.; I. Thomann,; Hollberg, L. & Diddams, S. A. (2004), *Opt. Lett.* 29, 403-405.

Baudelet, M.; Guyon, L.; Yu, J.; Wolf, J.-P.; Amodeo, T.; Frejafon, E. & Laloi, P. (2006). *Appl. Phys. Lett.* 88, 063901.

Baum, P. & Zewail, A. H. (2007). *PNAS* 104, 18409–18414.

Butkus, R.; Danielius, R.; Dubietis, A.; Piskarskas, A. & Stabinis, A. (2004). *Appl. Phys. B* 79, 693–700.

Cavalieri, A. L.; Müller, N.; Uphues, Th.; Yakovlev, V. S.; Baltuka, A.; Horvath, B.; Schmidt, B.; Blümel, L.; Holzwarth, R.; Hendel, S.; Drescher, M.; Kleineberg, U.; Echenique, P. M.; Kienberger, R.; Krausz, F. & Heinzmann, U. (2007), *Nature* 449, 1029-1032.

Chen, L.P.; Wang, Y. & Liu, J.M. (1996). *IEEE J. Quantum Electron.* 32, 1817.

Chen, Y.; Jiang, J. & Jones, D. J. (2006). *Opt. Express* 14, 12134-12144.

Corkum, P. B. & Krausz, F. (2007). *Nature Physics* 3, 381 – 387.

Crooker, S.A.; Betz, F.D.; Levy, J. & Awschalom, D.D. (1996). *Rev. Sci. Instrum.* 67, 2068.

De Barros, M. R. X. & Becker, P. C. (1993). *Opt. Lett.* 18, 631–633.

De Barros, M. R. X.; Miranda, R. S.; Jedju, T. M. & Becker, P. C. (1995), *Opt. Lett.* 20, 480.

Drescher, M.; Hentschel, M.; Kienberger, R.; Uiberacker, M.; Yakovlev, V.; Scrinzi, A.; Westerwalbesloh, Th.; Kleineberg, U.; Heinzmann, U. & Krausz, F. (2002). *Nature* 419, 803-807.

Eliyahu, D.; Salvatore, R.A. & Yariv, A. (1997). *J. Opt. Soc. Am. B* 14, 167.

Evans, J. M.; Spence, D. E.; Burns, D. & Sibbett, W. (1993). *Opt. Lett.* 18, 1074–1076.

Fekete, J.; Cserteg,A.& Szipocs, R. (2009). *Laser Phys. Lett.* 6, 49-53.

Fermann, M.E.; Galvanauskas, A.; Sucha1 G. & Harter, D. (1997). *Appl. Phys. B* 65, 259-275.

Fleischer, A. & Moiseyev, N. (2006). *Phys. Rev. A* 74 (5), 053806.

Foreman, S.M.; Holman, K.W.; Hudson, D. D.; Jones, D. J. & Ye, J. (2007). *Rev. Sci. Instrum.* 78, 021101.

Fuerst, C.; Leitenstorfer, A. & Laubereau, A. (1996). *IEEE J. Sel. Top. Quantum Electron.* 2, 473–479.

Goulielmakis, E.; Yakovlev, V. S. Cavalieri, A. L.; Uiberacker, M.; Pervak, V.; Apolonski, A.; Kienberger, R.; Kleineberg U.; & Krausz, F. (2007). *Science* 317, 769-775.

Gu, X.; Li, Pan, Y. H.; Wu, E. & Zeng, H. (2010). *IEEE J. Sel. Topics Quantum Electron.*, in press.

Hannaford, P. *Femtosecond Laser Spectroscopy* (Springer, New York, 2005) ISBN 0-387-23293-1.

Hao, Q.; Li, W. & Zeng, H. (2007) *Opt. Express* 15, 16754-16759.

Haus, H.A. & Mecozzi, A. (1993). *IEEE J. Quant. Elect.* QE-29, 983.

Hentschel, M.; Kienberger, R.; Spielmann, Ch.; Reider, G. A.; Milosevic, N.; Brabec, T.; Corkum, P.; Heinzmann, U.; Drescher M. & Krausz F. (2001). *Nature* 414, 509-513.

Hönninger, C.; Paschotta, R.; Morier-Genoud, F.; Moser, M. & Keller, U. (1999). *J. Opt. Soc. Am. B* 16, 46.

Jiang, L.A.; Wong S.T. & Grein, M.E. (2002). *IEEE J. Quantum Electron.* 38, 1047-1052.

Jones, D. J.; Diddams, S. A.; Ranka, J. K.; Stentz, A.; Windeler, R. S.; Hall, J. L. & Cundiff, S. T. (2000). *Science* 288, 635–639.

Jones, D. J.; Potma, E. O.; Cheng, J.; Burfeindt, B.; Pang, Y.; Ye, J. & Xie, X. S. (2002), *Rev. Sci. Instrum.* 73, 2843.

Kaindl, R. A.; Wurm, M.; Reimann, K.; Hamm, P.; Weiner, A. M. & Woerner, M. (2000). *J. Opt. Soc. Am. B* 17, 2086–2094.

Kawamura, K.; Ogawa, T.; Sarukura, N.; Hirano, M. & Hosono, H. (2000). *Appl. Phys. B* 71, 119–121.

Kienberger, R.; Hentschel, M.; Uiberacker, M.; Spielmann, Ch.; Kitzler, M.; Scrinzi, A.; Wieland, M.; Westerwalbesloh, Th.; Kleineberg, U.; Heinzmann, U.; Drescher, M. & Krausz, F. (2002). *Science* 297, 1144-1148.

Kitaeva, G. K. (2008). *Laser Phys. Lett.* 5, 559–576.

Kitzler, M.; Milosevic, N.; Scrinzi, A.; Krausz, F. & Brabec, T. (2002). *Phys. Rev. Lett.* 88 (17), 173904.

Kodama, R.; Norreys, P.A.; Mima, K.; Dangor, A.E.; Evans, R.G.; Fujita, H.; Kitagawa, Y.; Krushelnick, K.; Miyakoshi, T.; Miyanaga, N.; Norimatsu, T.; Rose, S.J.; Shozaki, T.; Shigemori, K.; Sunahara, A.; Tampo, M.; Tanaka, K.A.; Toyama, Y.; Yamanaka, T. & Zepf, M. (2001). *Nature* 412, 798–802.

a. Li, Y.; Li, W.; Hao, Q.; Yan, M.; Zhou, H. & Zeng, H. (2009). *Laser Phys. Lett.* DOI 10.1002, 1–5.

b. Li, Y.; Gu, X.; Yan, M.; Wu, E & Zeng, H. (2009). *Opt. Express* 17, 4526–4531.

a. Limpert, J.; Liem, A. Zellmer,; H. & Tünnemann, A. (2003). *Electron. Lett.* 39, 645-647.

b. Limpert, J.; Schreiber, T.; Liem, A.; Nolte, S.; Zellmer, H.; Peschel, T.; Guyenot, V. & Tünnermann, A. (2003). *Opt. Express* 11, 2982-2990.

c. Limpert, J.; Schreiber, T.; Nolte, S.; Zellmer, H.; Tünnermann, A.; Iliew, R.; Lederer, F.; Broeng, J.; Vienne, G.; Petersson,A. & Jakobsen, C. (2003). *Opt. Express* 11, 818-823.

Lisak, M.; Hook, A. & Anderson, X. (1990). *J. Opt. Soc. Am. B* 7, 810–814.

López-Martens, R.; Varjú, K.; Johnsson, P.; Mauritsson, J.; Mairesse, Y.; Salières, P; Gaarde, M. B.; Schafer, K. J.; Persson, A.; Svanberg, S.; Wahlström, C. & L'Huillier, A. (2005), *Phys. Rev. Lett.* 94, 033001.

Ma, L.-S.; Bi, Z.; Bartels, A.; Robertsson, L.; Zucco, M.; Windeler, R. S.; Wilpers, G.; Oates, C.; Hollberg, L. & Diddams S. A. (2004). *Science* 303, 1843-1845.

Manzoni, C.; Polli, D. & Cerullo, G. (2006), *Rev. Sci. Instrum.* 77, 023103.

Matsas, V. J.; Newson, T. P. & Zervas, M. N. (1992). *Opt. Commun.* 92, 61-66.

Mauritsson, J.; Johnsson, P.; Gustafsson, E.; L'Huillier, A.; Schafer,K. J. & Gaarde, M. B. (2006). *Phys. Rev. Lett.* 97, 013001.

Papadopoulos, D. N.; Zaouter, Y.; Hanna, M.; Druon, F.; Mottay, E.; Cormier, E. & Georges, P. (2007). *Opt. Lett.* 32, 2520-2522.

Paschotta, R. (2004). *Appl. Phys. B* 79, 163–173.
Potma, E.O.; Jones, D.J.; Cheng, J.-X.; Xie, X.S. & Ye, J. (2002). *Opt. Lett.* 27, 1168–1170.
Rudd, J.V.; Law, R.J.; Luk, T.S.; & Cameron, S.M. (2005). *Opt. Lett.* 30, 1974–1976.
Rullière, C. *Femtosecond laser pulses: principles and experiments, 2nd ed.* (Springer, New York, 2005) ISBN 978-0-387-01769-3.
a. Rusu, M.; Herda, R. & Okhotnikov, O. G. (2004). Optics Express 12(20), 4719-4724.
b. Rusu, M.; Herda R. and Okhotnikov, O. G. (2004) *Opt. Lett*. 29, 2246-2248.
Sansone, G.; Benedetti, E.; Calegari, F.; Vozzi, C.; Avaldi, L.; Flammini, R.; Poletto, L.; Villoresi, P.; Altucci, C.; Velotta, R.; Stagira1, S.; De Silvestri, S. & Nisoli, M. (2006). *Science* 314, 443-446.
Schoenlein, R. W.; Chattopadhyay, S.; Chong, H. H. W.; Glover, T. E.; Heimann, P. A.; Shank, C. V.; Zholents, A. A. & Zolotorev, M. S. (2000) *Science* 287, 2237-2240.
Shelton, R. K.; Ma, L.-S.; Kapteyn, H. C.; Murnane, M. M.; Hall, J. L. & Ye, J. (2001) *Science* 293, 1286-1289.
Schibli, T.R.; Kim, J.; Kuzucu, O.; Gopinath, J.T.; Tandon, S.N.; Petrich, G.S.; Kolodziejski, L.A.; Fujimoto, J.G.; Ippen, E.P. & Kaertner, F.X. (2003). *Opt. Lett.* 28, 947–949.
Schibli, T.R.; Minoshima, K.; Hong, F.-L.; Inaba, H.; Onae, A.; Matsumoto, H.; Hartl, I. & Fermann, M. E. (2004). *Opt. Lett.* 29, 2467-2469.
Schoenlein, R. W.; Leemans, W. P.; Chin, A. H.; Volfbeyn, P.; Glover, T. E.; Balling, P.; Zolotorev, M.; Kim, K.-J.; Chattopadhyay, S. & Shank, C. V. (1996). *Science* 274, 236–238.
a. Sell, A.; Leitenstorfer, A. & Huber, R. (2008). *Opt. Lett.* 33, 2767–2769.
b. Sell, A.; Scheu, R.; Leitenstorfer, A.; & Huber, R. (2008). *Appl. Phys. Lett.* 93, 251107.
Shelton, R.K.; Ma, L.-S.; Kapteyn, H.C.; Murnane, M.M.; Hall, J.L.; & Ye, J. (2001). *Science* 293, 1286–1289.
Shelton, R.K.; Foreman, S.M.; Ma, L.-S.; Hall, J.L.; Kapteyn, H.C.; Murnane, M.M.; Notcutt, M. & Ye, J. (2002). *Opt. Lett.* 27,312–314.
Shirakawa, A.; Sakane, I.; Takasaka, M. & Kobayashi, T. (1999). *Appl. Phys. Lett.* 74, 2268.
Son, D. H.; Kambhampati, P.; Kee, T. W. & Barbara, P. F. (2002), *J. Phys. Chem. A* 106, 4591–4597.
Spence, D.E.; Sleat, W.E.; Evans, J.M.; Sibbett, W. & Kafka, J.D. (1993). *Opt. Commun.* 101, 286.
Supradeepa, V. R.; Huang, C.; Leaird, D. E. & Weiner, A. M. (2008), *Opt. Express* 16, 11878-11887.
Telle, H. R.; Steinmeyer, G.; Dunlop, A. E.; Stenger, J.; Sutter, D. H. & Keller, U. (1999). *Appl. Phys. B* 69, 327–332.
Tong, X. M.; Zhao, Z. X. & Lin, C. D. (2003). *Phys. Rev. Lett.* 91, 233203.
Udem, Th.; Holzwarth, R. & Hänsch, T. W. (2002), *Nature* 416, 233-237.
Vozzi, C.; Calegari, F.; Ferrari, F.; Lucchini, M.; De Silvestri, S.; Svelto, O.; Sansone, G.; Stagira, S. & Nisoli, M. (2009). *Laser Phys. Lett.* 6, 259–267.
Wei, Z.; Kaboyashi Y. & Torizuka, K. (2002). *Appl. Phys. B* 74, S171–S176.
Wilcox, K.G.; Foreman, H.D.; Roberts J.S. & Tropper, A.C. (2006). *IEEE Electronic Lett.* 42, 1-3.
Xu, L.; Spielmann, C.; Krausz, F. & Szipöcs R. (1996). *Opt. Lett.* 21, 1259-1261.
a. Yan, M.; Li, W.; Hao, Q.; Li, Y. & Zeng H. (2009). *Opt. Lett.* 34, 2018–2020.

b. Yan, M.; Li, W.; Hao, Q.; Li, Y.; Yang, K.; Zhou H. & Zeng, H. (2009). *Opt. Lett.* 34, 3331–3333.

Yoshitomi, D.; Kobayashi, Y.; Takada, H.; Kakehata, M. & Torizuka, K. (2005). *Opt. Lett.* 30, 1408–1410.

Yoshitomi, D.; Kobayashi, Y.; Kakehata, M.; Takada, H.; Torizuka, K.; Onuma, T.; Yokoi, H.; Sekiguchi,T. & Nakamura, S. (2006). *Opt. Lett.* 31, 3243–3245.

Zhang, X.M.; Fan, D.Y.; Zeng, X.M.; Wei, X.F.; Huang, X.J.; Wang, X.; Zhu, Q.H. & Qian, L.J. (2006). *Opt. Lett.* 31, 646–648.

Zhu, C.; Wang, Y.; He, J.; Wang, S. & Hou, X. (2005). *J. Opt. Soc. Am. B* 22, 1221-1227.

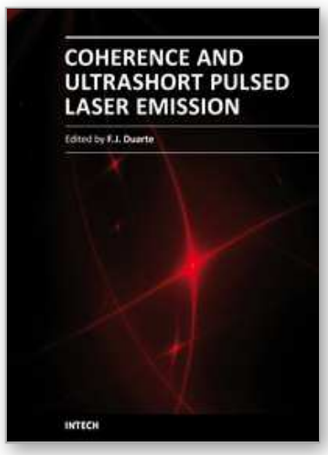

Coherence and Ultrashort Pulse Laser Emission

Edited by Dr. F. J. Duarte

ISBN 978-953-307-242-5
Hard cover, 688 pages
Publisher InTech
Published online 30, November, 2010
Published in print edition November, 2010

In this volume, recent contributions on coherence provide a useful perspective on the diversity of various coherent sources of emission and coherent related phenomena of current interest. These papers provide a preamble for a larger collection of contributions on ultrashort pulse laser generation and ultrashort pulse laser phenomena. Papers on ultrashort pulse phenomena include works on few cycle pulses, high-power generation, propagation in various media, to various applications of current interest. Undoubtedly, Coherence and Ultrashort Pulse Emission offers a rich and practical perspective on this rapidly evolving field.

How to reference

In order to correctly reference this scholarly work, feel free to copy and paste the following:

Wenxue Li, Qiang Hao, Yao Li, Ming Yan, Hui Zhou and Heping Zeng (2010). Ultrafast Laser Pulse Synchronization, Coherence and Ultrashort Pulse Laser Emission, Dr. F. J. Duarte (Ed.), ISBN: 978-953-307-242-5, InTech, Available from: http://www.intechopen.com/books/coherence-and-ultrashort-pulse-laser-emission/ultrafast-laser-pulse-synchronization

INTECH
open science | open minds

InTech Europe
University Campus STeP Ri
Slavka Krautzeka 83/A
51000 Rijeka, Croatia
Phone: +385 (51) 770 447
Fax: +385 (51) 686 166
www.intechopen.com

InTech China
Unit 405, Office Block, Hotel Equatorial Shanghai
No.65, Yan An Road (West), Shanghai, 200040, China
中国上海市延安西路65号上海国际贵都大饭店办公楼405单元
Phone: +86-21-62489820
Fax: +86-21-62489821

IntechOpen